ASSESSING THE DIURNAL CYCLE OF SURFACE ENERGY AND WATER FLUXES IN AN IRRIGATED AGRICULTURAL FIELD USING A HYDROLOGICAL MODEL

by

ROJINA MANANDHAR

Date: 27 April, 2007

Approved: 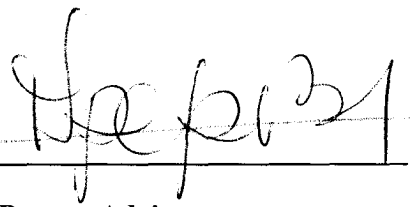

Dr. Ana P. Barros, Advisor

Masters project submitted in partial fulfillment of the requirements for the Master of Environmental Management Degree in the Nicholas School of the Environment and Earth Sciences of Duke University

2007

ABSTRACT

The diurnal variation of water and energy fluxes at the land surface is important to understand the diurnal cycle of photosynthesis, moisture and temperature at surface and deeper soil layers, especially during the growing season. The objective of the paper is to characterize the diurnal cycle of surface water and energy fluxes during the growing season of a corn in an irrigated agricultural field. The paper aims to study the response of the land-surface to observed atmospheric forcing at Citra, Florida, using a 1D column implementation of an existing land surface hydrology model.

The observational data are analyzed first, including a careful analysis of physical consistency and measurement error. Particular emphasis is placed on the steps taken to evaluate and improve the quality of the two key physical forcing for the model: observed precipitation and radiation forcing. Simulations of energy fluxes, soil moisture and soil temperature from the model are compared against observations at fifteen minute time scales.

The model is able to reproduce diurnal variability of the soil moisture and temperature in response to applied forcing. Root mean square error for soil moisture is calculated to be 0.033 m^3/m^3, 0.04 m^3/m^3, and 0.005 m^3/m^3 for superficial, middle and deeper layers respectively. A sensitivity study is conducted to investigate model behavior by changing thermal diffusivity and hydraulic diffusivity (not specified in the observation data), while keeping all other boundary conditions and physical forcing constant in the model. As opposed to previous applications with the model (at larger field scales and not for agricultural fields), it was found that thermal diffusivity and hydraulic diffusivity have a strong impact on the partitioning of the surface energy fluxes, especially in the case of thermal diffusivity with regard to diurnal variation of deep soil temperature.

ACKNOWLEDGEMENTS

My sincere appreciation goes to my project advisor Dr. Ana Barros, faculty at Pratt School of Engineering, Duke, for her meticulous guidance in carrying out the research and being a constant source of inspiration. I would like to extend my gratitude to my academic advisor Paul Baker for his encouragement, Dr. Shanti Bhushan, a past post doctorate with Dr. Barros, who advised me in early phase of my project, and scientists who were involved in Micro-WEX II experiment, especially, Jasmeet Judge, who were kind enough to provide me with their field data for carrying out my research. Lastly, many thanks to my friends and family, and my husband Prabhakar Shrestha, for always being there for me.

TABLE OF CONTENTS

CONTENTS **PAGE**

1. INTRODUCTION 5

2. OBJECTIVE 7

3. METHOD 8

3.1 Land Surface Hydrology Model description 8

3.2 Study Site characteristics and Measurement 16

4. CHARACTERIZATION OF UNCERTAINTY AND INCONSISTENCY IN OBSERVATION 19

4.1 Characterization of uncertainty in precipitation observations 19

4.2 Characterization of Uncertainty in the Radiation Forcing 21

4.3 Characterization of the inconsistency in the observation of energy fluxes 21

5. RESULTS AND DISCUSSION 28

5.1 Assessment of model transferability 28

5.2 Model Sensitivity to Thermal diffusivity and Hydraulic Diffusivity 37

6. CONCLUSIONS 46

7. REFERENCES 48

8. APPENDIX 52

1. INTRODUCTION

We often do not realize but changes in land surface processes due to human activities such as agriculture can have significant bearing on land atmosphere interactions, and hence determining a local climate in the region. Hydrological models are extensively used as research tools in characterizing the land atmosphere interactions at the land surface. The interaction is critically dependent on the physical properties of soils and vegetation as well as atmospheric conditions during the alternate periods of precipitation and evapotranspiration (Eagleson, 1978; Sellers, 1991). Vegetation changes and soil atmosphere dynamics induce diurnal variation in soil moisture and temperature gradients at surface and deeper layers of the soil. Garcia-Quizano and Barros (2005) and Gebremichael and Barros (2005) showed that the interaction of biophysical and hydrological processes is a key in capturing the diurnal cycle of evapotranspiration and photosynthesis, which are interconnected. Gebremichael and Barros (2005) demonstrated that the actual diurnal cycle of photosynthesis, (the measure of gross primary productivity), is determined by the interaction of radiative, meteorological and hydrological controls. The diurnal variation of water and energy fluxes at the land surface is thus important to understand the diurnal cycle of photosynthesis, moisture and temperature at surface and deeper soil layers, especially during the growing season.

At the land surface, soil and vegetation systems respond dynamically to precipitation and evapotranspiration events and play a major role in partitioning the surface energy into sensible heat and latent heat (Yildiz, 2001). In addition, availability of soil moisture at different depths in the soil column controls the partitioning of the two key energy fluxes, sensible and latent heat fluxes, in the model (Gutmann and Small, 2005). Garcia-Quijano and Barros (2005) showed that vegetation modulates climate variability through soil-vegetation-

atmosphere interactions. Vegetation controls surface-subsurface interactions via evapotranspiration which affects both the surface energy budget (and soil temperature) and water storage (soil moisture) in the root-zone, and therefore impacts rainfall-runoff response and potentially the overall hydrological regime of river basins and water resources (Falkenmark 1997).

In agricultural fields, there are two ways in which water stress affects plant productivity during the growing season: (1) via atmospheric evaporative demand, and (2) via soil water stress effects on photosynthesis. Numerical experiments suggest that soil moisture controls of the distribution of water potential from the root to the leaf level may have a more important role in photosynthesis than the impact of environmental evaporative demand on stomatal conductance (Garcia-Quijano and Barros, 2005; Gebremichael and Barros, 2005). This matter of mutual dependence among vegetation and hydrological processes has been investigated in a variety of modeling studies. For example, Xu et al. (2002) found that in forested landscapes, the diurnal pattern of surface soil moisture and temperature showed larger variability during the daytime when photosynthesis takes place rather than at night. Kahan, D.S. et al. (2005) showed that a combination of vegetation parameters (e.g. Leaf Area Index (LAI), stomatal resistance) and soil parameters such as saturated hydraulic conductivity are equally important to simulate latent heat and sensible heat fluxes, especially during daylight hours in arid regions. Along with strong moisture gradients, Hornbuckle and England (2005) found temperature differences as large as 10K between the surface and 4.5 cm depth beneath the maize canopy over the course of the growing season.

The primary focus of this study is to investigate the diurnal cycle of energy and water fluxes during the growing season of corn in a managed agricultural field in Florida using a

land surface hydrology model (LSHM). This physical based model was originally developed by Barros (1995). The model has been modified (Devonec and Barros, 2001), coupled with other models such as a vegetation dynamics and ground water flow, and has been tested in different regions (Devonec and Barros, 2002; Garcia-Quizano and Barros, 2005; Yildiz and Barros, 2005). The column version of LSHM simulates energy and moisture transport in soil and quantifies the energy and water fluxes at the land surface. Devonec and Barros (2002) verified the energy balance scheme of the land surface model at daily and seasonal time scales at Cabauw, and for the continental US using two years of data from the International Satellite and Surface Climatology Project (ISLSCP) Initiative I data set (ISLSCP-Halls and Sellers, 1995). Yildiz and Barros (2005) studied in detail the propagation of uncertainty in LSHM, from rainfall, a key forcing in the model, and showed that it varies spatially with the physical processes that control local rainfall-runoff response. Although Garcia-Quijano and Barros (2005) and Gebremichael and Barros (2005) used a column version of the model equipped with a biophysics module, in this study we will follow Devonec and Barros (2002) who used the uncoupled hydrology model and specified time-varying vegetation parameters in the model (LAI, Fractional vegetation cover) at every time-step.

2. OBJECTIVE

The primary objective of this research was to understand the diurnal cycle of land atmosphere interactions during the crop growing season in an irrigated agricultural field. In particular, we intended to investigate diurnal variation of soil moisture and temperature profiles in response to precipitation and irrigation, and how the diurnal cycle changes during the growing season.

The objective was accomplished by 1) initializing the land surface model with physical conditions of the experimental site 2) simulating the energy fluxes and soil moisture and temperature with measured atmospheric forcing dataset 3) evaluating the transferability of model in capturing the diurnal response by comparing the results with the observation records.

3. METHOD

3.1 Land Surface Hydrology Model description

3.1.1 Introduction

The 1D version of the land-surface hydrology model consists of two major components: an energy balance model and a water balance model (Appendix. 1). The purpose of the model is to simulate the hydrologic processes at the land surface interface and in the upper soil layers down to the ground water table, and to quantify energy and water fluxes when atmospheric forcing is provided.

The conceptual model consists of an atmospheric boundary layer column and a soil column. The vertical soil column consists of a minimum of three discrete layers involved in soil water and heat transfer mechanisms. An upper thin superficial layer functions as the interface between the ground and atmosphere and supplies water to deeper soil layers. An intermediate layer extends through the upper and lower root zones; and the deeper layer extends between the root zone and the local water table, or alternately impermeable boundary, that produces base flow.

At the land surface, available water is partitioned among four reservoirs: bare soil, vegetated area, snow cover, and four distinct types of skin storage capacity, including dew formation on plant leaves or on bare soil surfaces, interception of rainfall by canopy, and

ponding on soil surface or on the snow pack during superficial melting. In this application of LSHM, the snow processes are not included because the simulations are for the summer season in Florida. A brief description of the model's formulation is presented next (Appendix 2 for flow chart).

3.1.2 Surface Energy balance

The surface energy balance can be described by:

$$C * h_0 \frac{\partial T_0}{\partial T} = (F_R + H + LE) + GH \quad (1)$$

where the left hand term represents change in heat storage in the superficial soil layer, F_R is the total radiative flux comprising net shortwave and long wave radiation, H is the sensible heat flux, LE is the latent heat flux, and GH is the ground heat flux, representing the heat conduction in the soil, calculated as follows:

$$GH = -C * h_d \frac{\partial T_d}{\partial t} \quad (2)$$

where C* represents the volumetric heat capacity of the land surface, T_d and T_0 are respectively the temperature of deep and superficial soil layers, and h_d and h_0 are thickness of deep and superficial soil layers respectively.

The total flux F_R consists of the contribution of net solar shortwave radiation F_s, outgoing long wave radiation emitted by the earth's surface F_{lo}, and incoming long wave radiation F_{li} originated from clouds, aerosols and greenhouse gases:

$$F_R = F_R + F_{li} + F_{lo} \quad (3)$$

The net solar radiation flux is equal to the downward incoming flux F_{si} minus the reflected fraction:

$$F_s = (1 - a_g) F_{si} \quad (4)$$

where a_g is the effective land surface albedo, taken as an areally weighted function of bare soil albedo (a_0) and vegetation albedo (a_v):

$$a_g = (1 - C_v) a_0 + C_v a_v \quad (5)$$

C_v represents the fractional grid covered by vegetation.

The long wave radiation is determined based on the Stefan-Boltzman radiative law for a grey body:

$$F_l = F_{li} - F_{lo} = \sigma(\varepsilon_a T_a^4 - \varepsilon_g T_0^4) \quad (6)$$

where ε_a and ε_g are the emissivities of atmosphere and ground surface, T_a and T_o are the air and ground temperatures (^{0}K), respectively and σ is the Stefan-Boltzmann constant ($WK^{-4}m^{-2}$).

The sensible and latent heat fluxes are expressed as follows:

$$S_h = C_p \rho_a C_H |U_1| (T_1 - T_0) \quad (7)$$

$$L_h = L_v \rho_a C_W |U_1| (q_1 - q_{sat}) \quad (8)$$

where the subscript 1 indicates a reference height in the boundary layer where the horizontal wind U_1, temperature T_1 and specific humidity q_1 are measured and have precise physical meaning. T_0 is the ground surface temperature; q_{sat} is the saturated vapor pressure at the ground surface; ρ_a is the density of the air; C_p is the heat capacity of air at constant pressure; L_v is the latent heat of water vaporization; and C_H and C_W are the heat and water aerodynamic drag coefficients respectively.

Louis (1979) derived a very simple numeric scheme for the parameterization of the aerodynamic drag coefficient K_H:

$$K_H = a\left\{1 - \left[\frac{bR_i}{1 + cR_i^{1/2}}\right]\right\} \tag{9a}$$

and

$$a = \frac{k^2}{\left[\ln\left[\frac{z}{z_r}\right]\right]^2} \tag{9b}$$

where z is the roughness height, and z_r is the reference height, R_i (z) is the bulk Richardson number, and b and c are coefficients depending on the stability conditions.

Mahrt and Sun [1995] suggested adding a 'sub grid velocity scale' to average wind velocity in order to account for sub grid mesoscale motions generating turbulent fluxes. The measured velocity profile, corrected by the addition of the sub grid velocity scale term V_{sg}:

$$U = U_1 + V_{sg} \tag{10a}$$

with

$$V_{sg} = k\left(\frac{g}{T_0}\Delta T \Delta x\right)^{1/2} \tag{10b}$$

where g is the gravity acceleration constant (9.8 ms^{-2}), T_0 is the surface temperature, ΔT is the measure of variation of surface temperature, Δx is the characteristic length scale (grid size in distributed models) , and k is a function of the wind speed U_1.

3.1.3 Surface water balance

The formulation consists of the identification of possible water reservoirs in the original land surface model, and subsequently, partitioning of the available water among those

reservoirs. In the original land surface model, four reservoirs are considered: bare soil, vegetated area, snow cover, and four distinct type of 'skin' storage capacity including dew formation on plant leaves or on bare soil surfaces, interception of rainfall by canopy, and ponding on the soil surface or on the snow pack during superficial melting.

3.1.4 Evaporation

The total evaporation E_t represents the combination of the partial evaporation fluxes from the vegetation, skin and bare soil:

$$E_t = E^{total}{}_{sk} + C_v E_v + (1 - C_v) E_b \tag{11}$$

where E_t, E_{sk} and E_v are total evaporation, skin evaporation, evapotranspiration, and bare soil evaporation respectively.

The skin evaporation is determined based on the classic Monin-Obukhov theory to estimate evaporation from a free surface of water:

$$E_{sk} = \rho_a C_H \, |U_1| \left[q_1 - q_{sat}(T_0, P_0) \right] \tag{12}$$

where ρ_a is density of the air. This flux is limited to the actual contents of the individual reservoirs.

Bare soil evaporation is calculated using a modified threshold approach by which the saturated specific humidity at the ground surface $q_{sat}(T_0,P_0)$ is multiplied by a correction factor f_w. This factor depends on the actual surface wetness W_0 and the soil wetness at saturation W_{sat}.

$$E_b = \rho_a C_W \, |U_1| \left[q_1 - f_w q_{sat}(T_0, P_0) \right] \tag{13a}$$

where f_w takes values between zero and one and defined as:

$$f_w = 0.5\left[1 - \cos \pi (W_0 / W_{sat})\right] \quad (13b)$$

Evapotranspiration is estimated based on the simplified Monteith formulation as proposed by Rowntree [1991]:

$$E_b = \rho_a \frac{q_1 - q_{sat}(T_0, P_0)}{r_a + r_c} \quad (14a)$$

where r_a is the aerodynamic resistance defined as follows:

$$r_c = \frac{r_{\min}}{U_1 C_H} \quad (14b)$$

and rc is the canopy resistance, which is the integral mean of the resistance of the individual leaves. At night time, $r_c = r_{min}$.

The relative conductance of plants as a function of moisture availability is expressed as:

$$G(W) = \frac{W - W_{wp}}{W_{fc} - W_{wp}} \quad (15a)$$

where W is the soil moisture contained in the root zone, W_{wp} is the wilting point, and W_{fc} is the field capacity. When the soil moisture is below the wilting point, plant resistance takes its maximum value and evaporation is practically shut off. The empirical equations that relate plant conductance to incoming solar radiation ($G(F_{si})$) and to temperature (G(T)) are obtained from Stewart [1988]:

$$G(F_{si}) = \frac{46255 F_{si}}{41870 F_{si} + 104.4} \quad (15b)$$

$$G(T) = \frac{T_0 (40 - T_0) 1.18}{691} \quad (15c)$$

where F_{si} is expressed in cal cm^{-2} s^{-1} and T_0 in degree centigrade.

3.1.5 Soil water transfer mechanisms

Three soil layers are involved in the soil water transfer mechanisms: (1) a superficial layer that functions as an interface with the atmosphere, produces bare soil evaporation, and supplies water to deeper layers, (2) an intermediate layer that extends throughout the root zone, and (3) a deep layer that produces base flow. The modified soil water transfer scheme among the three layers can be expressed as:

$$\frac{\partial W_0}{\partial T} = \frac{1}{\rho_w}(1 - C_v)E_b + 1 - G_{o,m} + \Phi_{diff_{m,o}} + \Phi_{Ru_0} \qquad (16a)$$

$$\frac{\partial W_m}{\partial T} = G_{o,m} - G_{m,d} - \phi_{diff_{m,o}} + \Phi_{diff_{m,o}} + \Phi_{Ru_0} \qquad (16b)$$

$$\frac{\partial W_d}{\partial T} = G_{m,d} - \Phi_{diffd,m} - G_{bf} \qquad (16c)$$

where W_0, W_m and W_d are the actual water contents in superficial, middle and deep layers respectively, measured in depth of water; the order of subscripts implies that the flux is directed from the first layer to the second; G is the gravity flux that drains water from an upper layer to deeper layer; Φ_{diff} is the diffusive flux that relates the two layers in either direction with the reference direction being the upper layer; Φ_{Ru} is the root uptake function for a given layer (note that it is negative, as the evaporation flux); I is the infiltration and G_{bf} is the subsurface baseflow. The maximum infiltration rate I_{max} is set equal to the saturated hydraulic conductivity.

The land surface model includes Campbell (1974) and Brooks and Corey (1964) parameterizations for gravity flux (G), which is expressed for a given layer as:

$$G = K_h \left(\frac{W}{W_{sat}} \right)^n \quad (17a)$$

and

$$G = K_h \left(\frac{W - W_{fc}}{W_{sat} - W_{fc}} \right)^n \quad (17b)$$

The exponent 'n' can be equal to one in which case the gravity flux varies linearly with soil moisture content, or can be defined as a function of the soil properties ($n=3+2/\lambda$) where λ is the pore size index (Rawls and Brakensiek, 1985). Overall, eqn 17a produces higher fluxes than eqn 17b as it allows for drainage to occur even when soil moisture is below field capacity.

The root uptake flux (Φ_{Ru}) is calculated when the moisture content of a soil layer is above the wilting point. The total root uptake is assumed to be equal to the transpiration. The superficial and intermediate layer root uptakes (Φ_{Ru0} and Φ_{Rum}) are calculated based on formulations from ECMWF (1991) as:

$$\phi_{Ru_0} = \frac{1}{\rho_w} \left(\frac{W_o^{\,2}}{W_0^{\,2} + W_m^{\,2}} \right) C_v E_v \quad (18a)$$

$$\phi_{Ru_m} = \frac{1}{\rho_w} \left(\frac{W_m^{\,2}}{W_0^{\,2} + W_m^{\,2}} \right) C_v E_v \quad (18b)$$

The diffusive flux (Φ_{diff}) between adjacent layers depends on the moisture gradient between the two layers. Thus, the diffusion fluxes between superficial and middle layers ($\Phi_{m,o}$) and middle and deep layer ($\Phi_{d,m}$) can be expressed as:

$$\phi_{diff\ m,o} = D_c\left(\frac{W_m - W_0}{W_{sat}}\right) \quad (19a)$$

$$\phi_{diff\ d,m} = D_c\left(\frac{W_d - W_m}{W_{sat}}\right) \quad (19b)$$

Where, D_c is the diffusion coefficient and varies linearly with the hydraulic conductivity.

3.2 Study Site characteristics and Measurement

The land-surface hydrological modeling was driven by atmospheric forcing data obtained from a MicroWEX-2 experiment conducted by the Center for Remote Sensing (CRS), University of Florida in an agricultural plot of sweet corn plants (variety Saturn SH2) located in the Plant Science Research and Education Unit (PSREU) in Citra, Florida (29.41 N, 82.18 W) [Appendix 3]. Data were available from March 15 through June 3, 2004 (Casanova et al. 2005*)*. The CRS Florida site consists of a 3.6 ha (9 acre) irrigated agricultural plot, instrumented with a ground based microwave radiometer system, and micrometeorological stations. The data set includes upward and downward short and long wave radiation (measured by CNR radiometers), air temperature, specific humidity of the air, wind speed at the height of 2.1m. Sensible and latent heat fluxes were estimated using Eddy-covariance system at 2.1m. The energy balance data are available with a fifteen minute time step from March 18 (DoY 78) through June 2, 2004 (DoY 154) during the growing season of corn. After May 5 (DoY 126), the fraction of vegetation growth was unity. The evolution of leaf area index and fraction vegetation coverage is shown in fig. 1. The data set also includes soil moisture and temperature measured at depths of 2, 4, 8, 16, 32, 64 and 100 cm within the same time interval. Four tipping bucket rain gauges recorded precipitation at four locations:

east and west edge of the radiometer footprint, and east and west side of the field [Appendix 4].

The LSHM was driven by these multiple input variables measured at the agricultural plot. The data were used to specify initial condition of soil moisture and temperature and to validate model's performance. The soil column in the land surface model was divided into three discrete layers for water and energy transfer mechanisms. The upper 10 cm layer acts as an interface between surface and atmosphere for energy balance. The second layer is an intermediate layer expanding throughout the root zone with a varying depth across the river basin as a function of land cover type. For the simulation, the intermediate layer was discretized into a middle layer of 35 cm. The third layer extends between root zone layer and the local water table and is set to the depth of 1 m. The lower boundary condition is specified as heat transfer. There were only five observations recorded for leaf area index (LAI) and fractional vegetation cover in four stations for the entire growing period. These observations were averaged and interpolated to fifteen minute time steps to describe the state of the vegetation.

Certain physical parameters, such as stomatal resistance, field capacity, wilting point, etc. required to force the model were estimated based on previous literatures, that best conform to the field environment. Typical values for minimum stomatal resistance for crops such as corn and soybean is found to vary from 25-50 sm^{-1} (Korner et al, 1979). A value of 40 sm^{-1} for minimum stomatal resistance was used in the model. A list of physical parameters used for forcing the model is summarized in Appendices 5a and 5b.

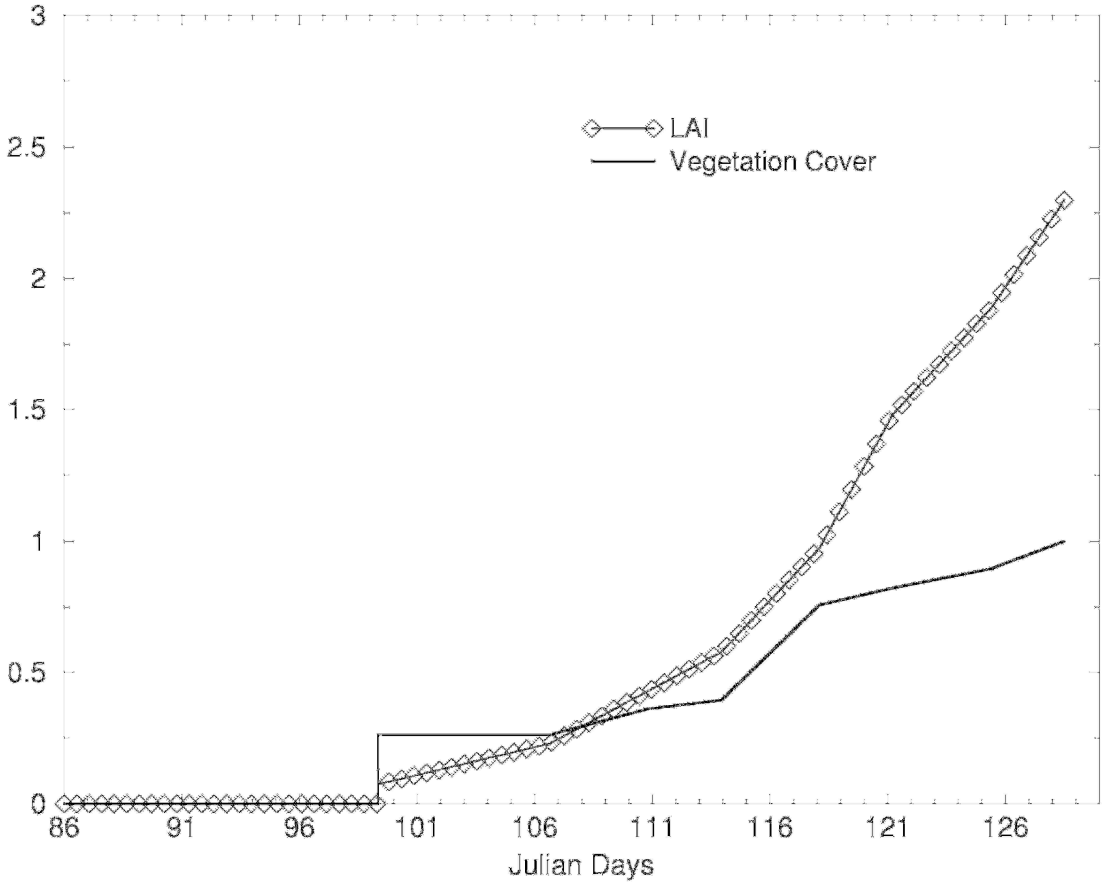

Fig. 1 Vegetation cover and Leaf Area Index, showing growth of corn, 2004 (originally recorded only for certain days, which has been interpolated to every fifteen minute time interval for this study)

4. CHARACTERIZATION OF UNCERTAINTY AND INCONSISTENCY IN OBSERVATION

For this study, the field observations can be divided into two classes: (1) forcing; and (2) evaluation. Soil moisture, soil temperature, and surface heat fluxes are in the latter category. Precipitation and incoming shortwave and long wave radiation are the key physical forcing along with boundary layer characteristics (wind, air temperature and relative humidity). Because of its importance for meaningful evaluation of model physics, a review of the steps taken to evaluate and improve the quality of the precipitation and radiation forcing is presented in this section. Also, steps were taken to check the consistency of the observation, primarily energy fluxes, for meaningful comparison of the results.

4.1 Characterization of uncertainty in precipitation observations

Precipitation is measured using four tipping bucket rain gages, two on either side of the footprint (25.1 ft * 30 ft) and two on either side of the field edge at a distance of 600 ft apart [Appendix 4]. In addition, the CRS site is irrigated and fertigated[1] at different times using different amounts. Besides the four rain gauge records, a daily time-series of precipitation including rainfall, irrigation and fertigation is also available (provided by Dr. Michael Dukes, University of Florida, and hereafter referred to as the Dukes' record). Rain gauges may not be sensitive enough to capture either irrigation or fertigation because these are typically characterized by very low intensities with very small drop sizes, conditions for which rain gauge measurements are known to exhibit severe under catch errors. Indeed, the records from the four rain gauges are not consistent with each other, or with the Dukes' record. None of the rain gauges appeared to capture irrigation and fertigation recorded by Dr.

[1] 'Fertigation' means application of fertilizer with water

Dukes for the entire period. Whereas it is expected that even nearby rain gauges may exhibit significant differences (Ciach, 2003) and that rain gauge measurement error is estimated to be 1-5% of the total catch (Winter, 1981), the key question is to determine which of the four rain gauges is closer to the actual rainfall.

The first step to minimize precipitation uncertainty was to estimate one aggregate rainfall time-series for the agricultural field. The rain gauges on the eastern foot print and the eastern field edge (about 400 ft apart, Appendix 5) capture significantly higher rainfall than the western stations (about 200 ft apart) [Fig. 2(a) and 2(b)]. Based on the precipitation distribution profile, a composite rainfall data set was created using the maximum values of precipitation recorded in eastern field edge and eastern foot print stations.

The second step was to downscale irrigation and fertigation from the Dukes' record into this aggregate precipitation data set. Since it was not possible to acquire tangible information regarding the daily distribution of irrigation and fertigation, the approach was to distribute the daily amounts according to the regional diurnal cycle of rainfall, thus at least guaranteeing that the composite record replicates the known climatology. Previous studies on the diurnal cycle of precipitation in north central Florida were used to distribute irrigation and fertigation in the agricultural field. Specifically, the diurnal cycle of precipitation from both the eastern field edge and the eastern foot print stations were compared with the diurnal variability of Florida rainfall recorded for the north central cities of Inglis ($29^0$02'N, $82^0$41'), Lynne ($29^0$10' N, $81^0$52'), and Daytona Beach ($29^0$11'N, $81^0$03') by Schwartz and Bozart (1979). The closer proximity of these cities to the experimental site in Florida ($29^0$41'N, $82^0$18'W) provided justification for application of the studies in this context. The diurnal cycle of precipitation recorded from the eastern field edge conforms better than the eastern

footprint with the diurnal variability observed in the three north central cities of Florida [Fig. 3]. The eastern field edge station was therefore selected for downscaling the Dukes' irrigation and fertigation records. For this purpose, the average diurnal cycle from the eastern field edge was normalized by the total precipitation and the normalized curve was used to distribute the irrigation and fertigation amounts, which were subsequently integrated with the composite rainfall record.

4.2 Characterization of Uncertainty in the Radiation Forcing

Shortwave and longwave radiation were measured by a REBS CNR net radiometer at the experimental site. Both these observations have missing data for certain time periods. Figure 4(a) provides a strong case of observational uncertainty in down welling shortwave radiation, in particular, for days 98 and 116. On the contrary, observations for DoY 92-98, and 105-111 [Fig. 4(b)] are coherent. Thus, these days are used for model evaluation, in the results section.

4.3 Characterization of the inconsistency in the observation of energy fluxes

The consistency of the observation was checked by evaluating energy budget closure. The comparison was done between net radiation calculated from basic energy balance equation (eqn 20a) and net radiation calculated from radiation forcing (eqn 20b):

$$R = LE + H + GH \qquad 20(a)$$

and

$$R = (1 - a_g)F_{si} + F_{li} - F_{lo} \qquad 20(b)$$

where R is the net radiation flux (w/m^{-2}), GH is the ground heat flux measured at 2 cm soil depth. A constant albedo of 0.25 was used.

The evaluation indicated inability to close the surface energy balance. The net energy calculated using eqns 20(a) and 20(b) was not strongly correlated [correlation of 0.62 for DoY 92-95, Fig. 5]. One of the potential issues, other than measurement uncertainty and missing observation characterized in down-welling radiation, could be attributed to uncertainty in the measurement of ground heat flux. Net radiation was partitioned to 19% of the ground heat flux between days 92-95 (daytime average). Jacobs et al (2002) study in prairie wetland under drought conditions in Paynes Prairie Preserve in north central Florida found that approximately 4% of the net radiation was partitioned to ground heat flux (daytime average) for the last week of May. Also, latent and sensible heat fluxes were estimated in the experimental site using eddy covariance method. Massman and Lee (2002) have indicated flux loss due to physical limitations of the eddy-covariance instrumentation. They discussed the underestimation of eddy-covariance fluxes due to inability to measure low frequency contributions, coordinate systems and nighttime flux measurements in their paper. Without some understanding of an ability to compensate for these observation uncertainties, the evaluation of model physics becomes difficult.

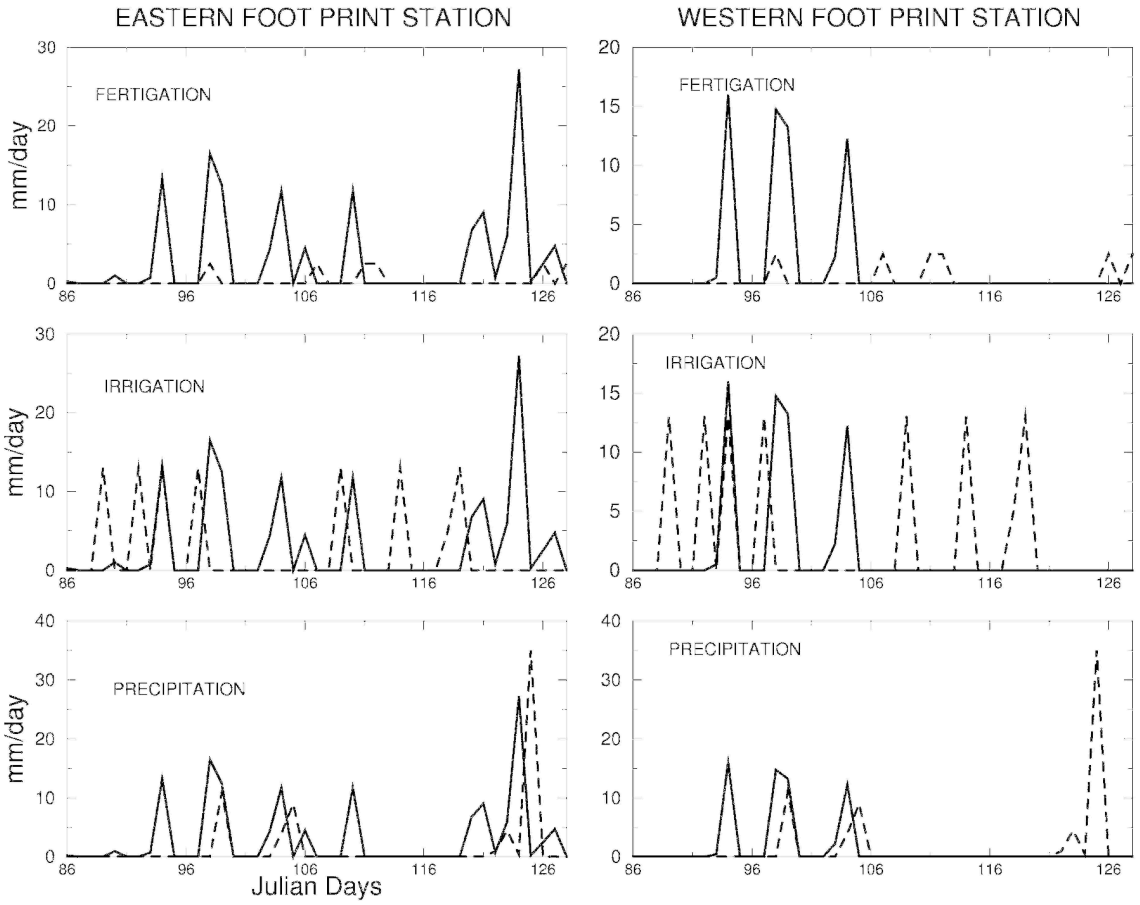

Fig. 2(a) Comparison of observed precipitation records in foot print station (eastern foot print on the left and western foot print on the right) with Dr. Dukes' daily record on fertigation, irrigation and precipitation (shown in dashed lines).

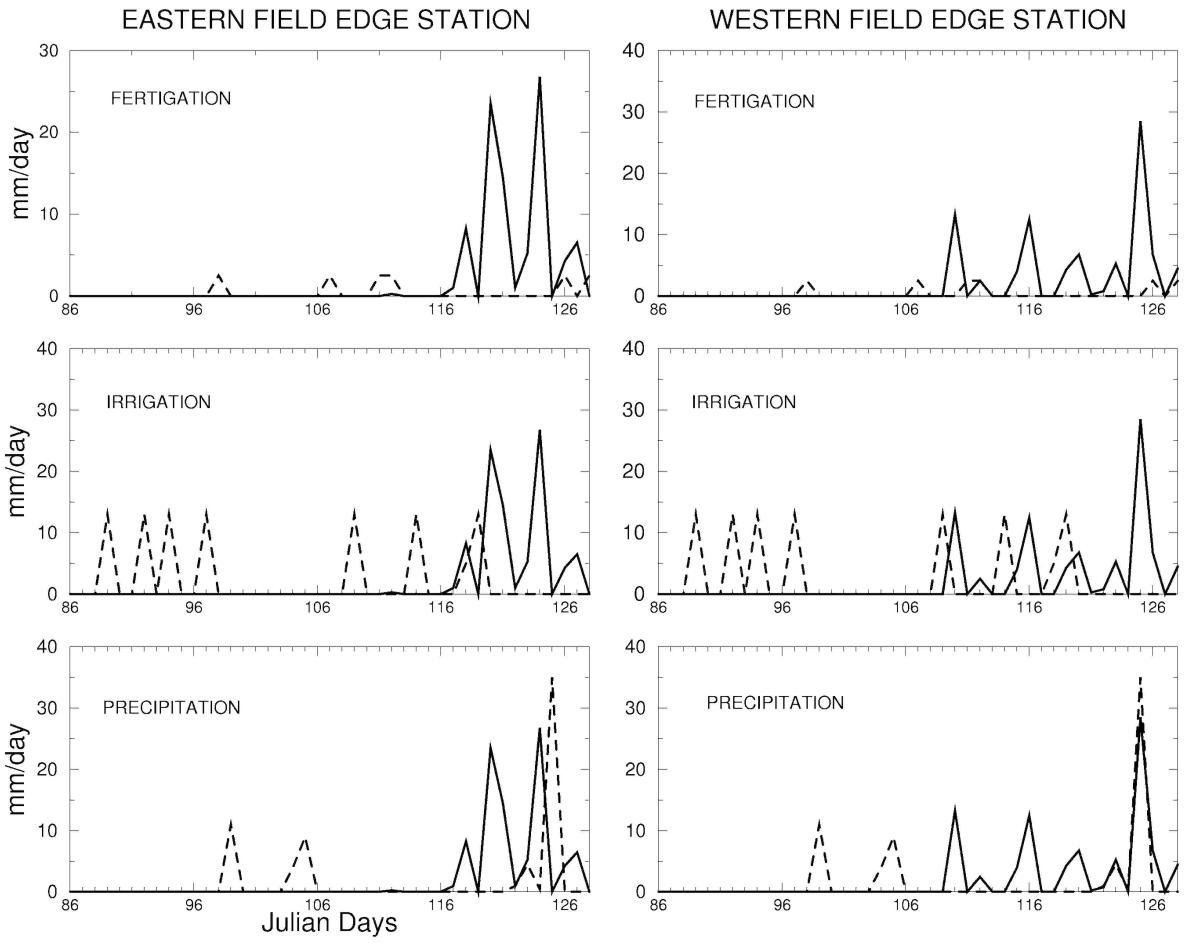

Fig. 2(b) Comparison of observed precipitation records in field edge stations (eastern field edge station on the left and western field edge on the right) with Dr. Dukes' daily record on fertigation, irrigation and precipitation (shown in dashed lines).

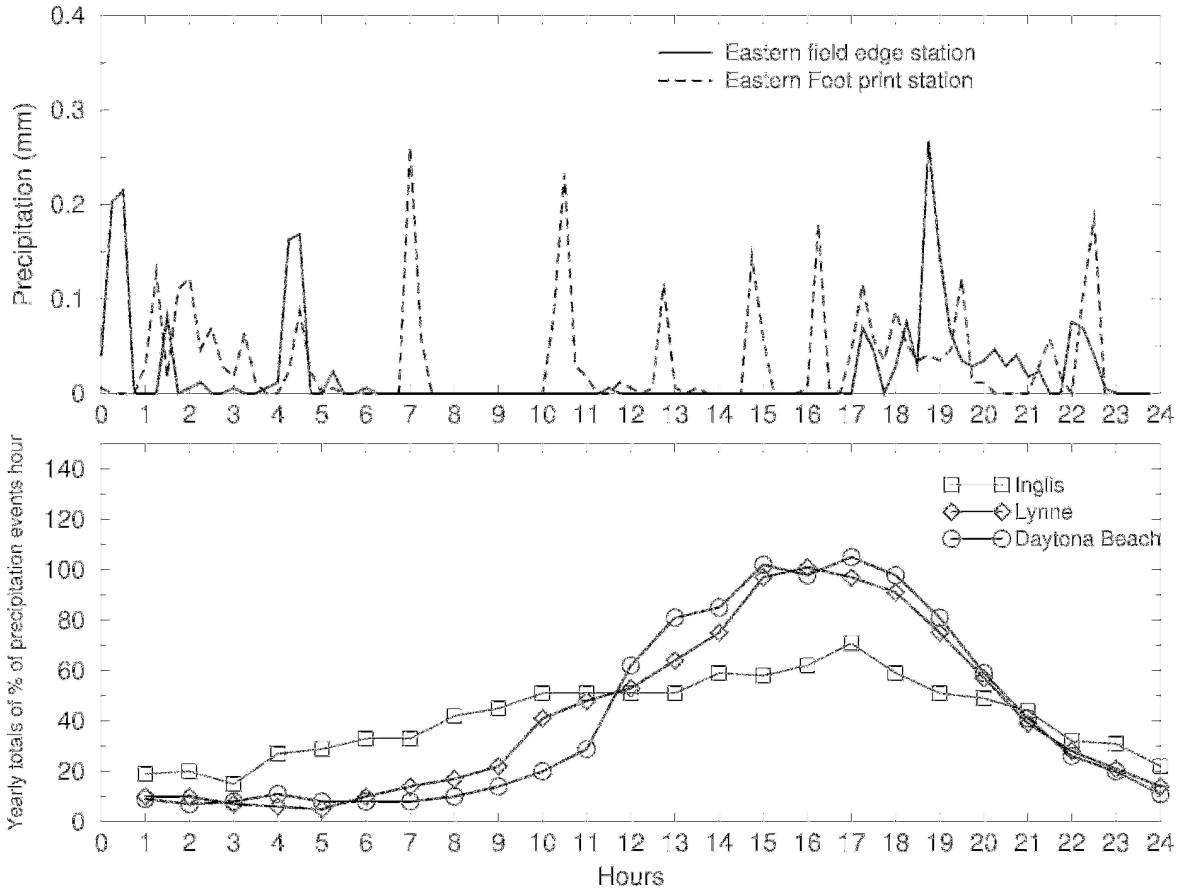

Fig.3. Comparison of diurnal precipitation recorded in eastern field edge and eastern footprint station with diurnal precipitation pattern studied in three north central cities of Florida (Schwartz and Bosart, 1979)

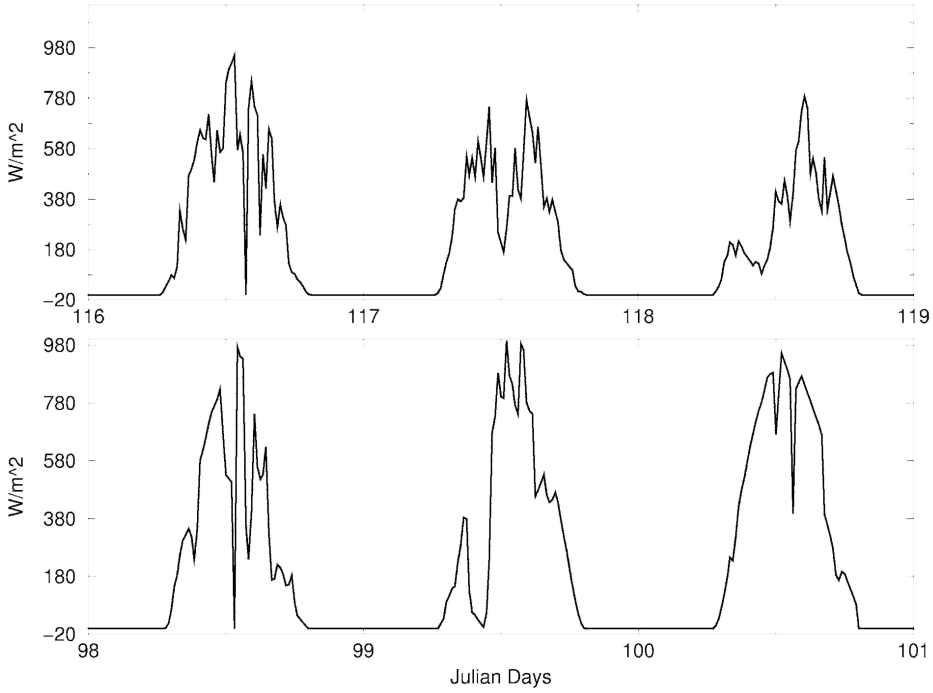

Fig 4(a) Measured down-welling shortwave radiation profile for days 116 -119 and 98 - 101.

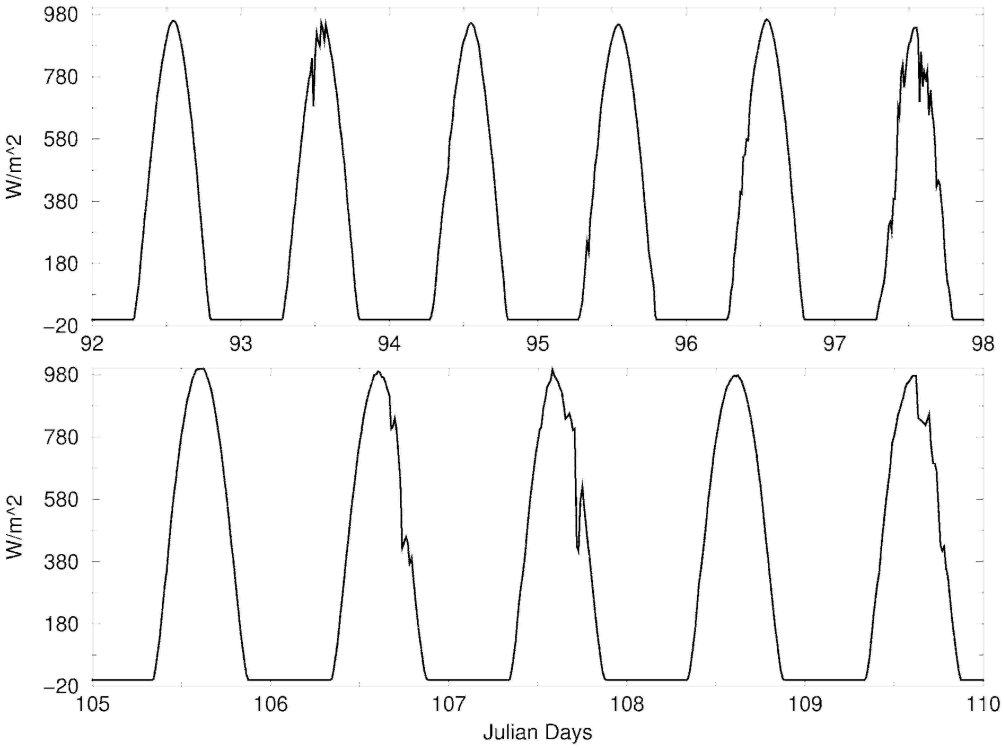

Fig 4(b) Measured down-welling shortwave radiation profile for days 92 -98 and 105-110, which appeared to be consistently accurate observations

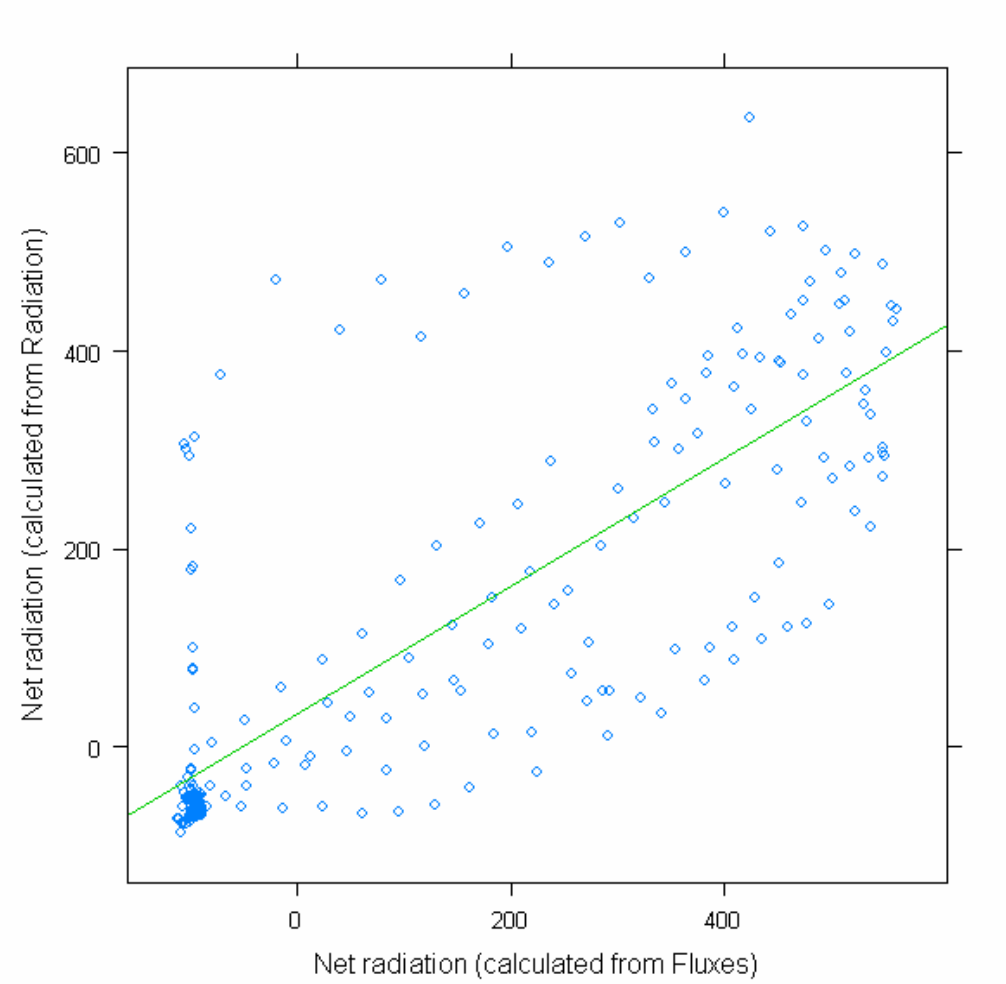

Fig 5. Comparison of net radiation calculated from measured energy fluxes against measured radiation forcing data set for days 92-95, giving regression coefficient (R^2) of 0.62, (green line indicates line of best fit).

5. RESULTS AND DISCUSSION

5.1 Assessment of model transferability

The performance of the model in capturing the diurnal cycle of energy and water fluxes was evaluated with the 15 minute CRS data set in the field. The simulation was started at DoY 86 (midnight, March 26). Soil moisture and temperature for all three discrete layers were initialized using the CRS data set at that time. The results are all based on one dimensional simulation output from LSHM. In all the first applications, thermal diffusivity is specified in the order of 10^{-8} and water diffusion in the soil in the order of 10^{-7}. The model sensitivity to both these parameters will be discussed in Section 5.2.

Energy fluxes

The well-defined diurnal pattern of simulated energy fluxes for the first week of April [Fig. 6], with a pronounced afternoon diurnal maximum, indicates that the model is well able to reproduce diurnal variability of the fluxes. The findings agree with the study done by Scwartz and Bosart (1979), which suggested that the greatest amplitude of the diurnal cycle appear further to the south during the spring season (March to May) with maximum midday diurnal in Florida (Schwartz and Bosart, 1979). The net radiation is partitioned to 3% of ground heat flux for the early growing season, while the rest makes up for the latent and sensible heat fluxes.

Latent heat flux

The weak regression coefficient of 0.49 between simulation and observation for days 86-92 [Fig. 7] indicates the possible uncertainty in eddy-covariance estimates of latent heat flux. The simulated latent heat flux compares well with the estimated data on the fifteen minute time interval for days 92 to 98 [Fig. 8a]. The overestimation of the simulated latent

heat flux for the first day is attributed to measurement data inaccuracy (missing observation on day 92). The consistent afternoon diurnal maximum indicates that the model is well able to reproduce a diurnal cycle of evapotranspiration. The average latent heat energy flux (41.37 W/m^2) compares well with the estimate (45.76 W/m^2) for those days, with root mean square error of 55.14 W/m^2. Since the simulation was done for the early growing season, latent heat flux was lower compared to sensible heat flux for most of the days.

Sensible heat flux

Comparison of diurnal variation of simulated and estimated sensible heat flux is presented in Fig. 8b. Sensible heat was estimated using an eddy-covariance system. Simulated sensible heat flux was computed by LSHM based on wind velocity and temperature gradient between soil surface and atmosphere at 2.1m height and constant roughness length. The model is able to capture the daily cycle of sensible heat flux but overestimates the observed heat flux. The root mean square error between the estimates and simulation is 99.55 W/m^2, with average sensible heat flux of 93.57 W/m^2 and estimated 43.54 W/m^2 for the days 92 to 98.

Model simulation of sensitive flux is greatly dependent on the estimation of aerodynamic transfer coefficient, which is based on the assumption of a logarithmic wind profile and a roughness length. Several studies (Anderson, 1976; Grimenes and Thue-Hansen, 2004) have found that roughness height decreases with plant growth. The model's sensible heat simulation was found to be sensitive to the selected values of roughness height in the range of 0.0015 and 0.30m (Eltayeb, 1997). The discrepancy in the sensible heat flux could be due to the constant value of the roughness parameter specified for this application.

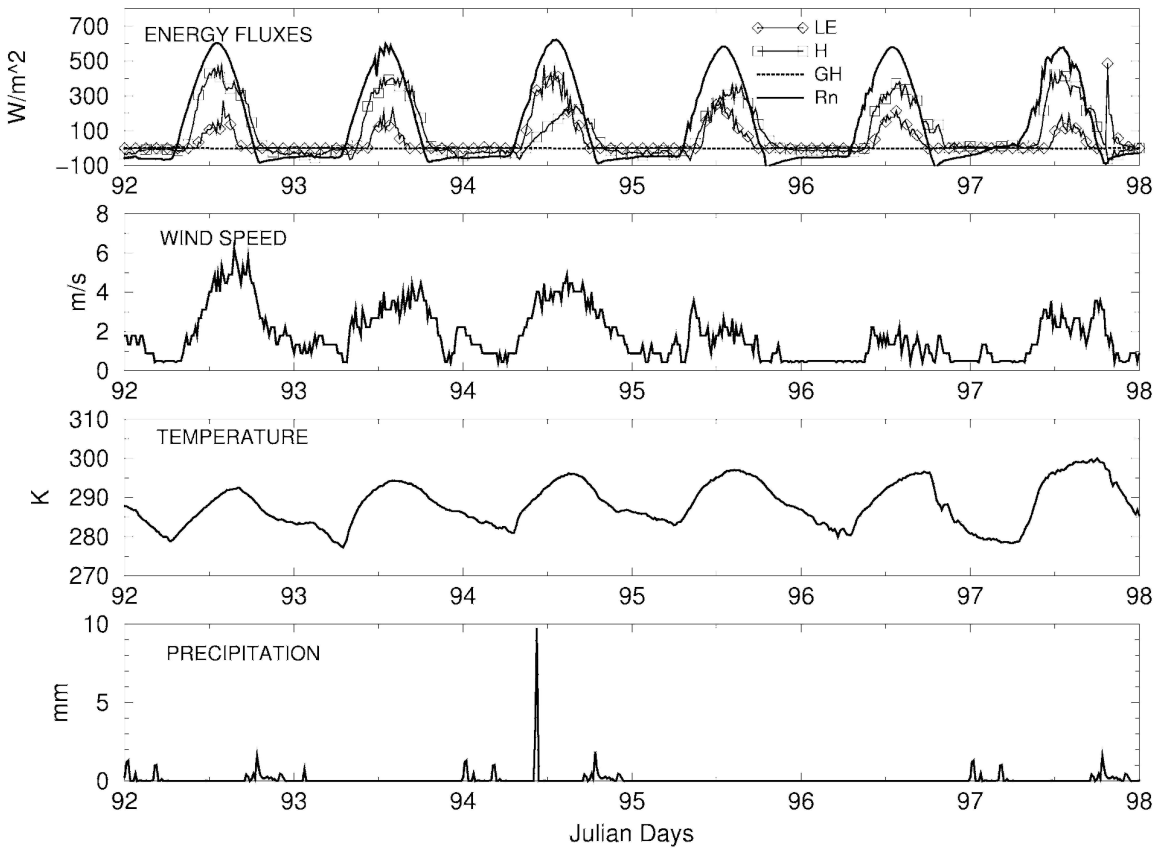

Fig.6. Simulated daily diurnal cycles of fluxes, measured wind speed, temperature and the corrected precipitation for first week of April (days 92-98)

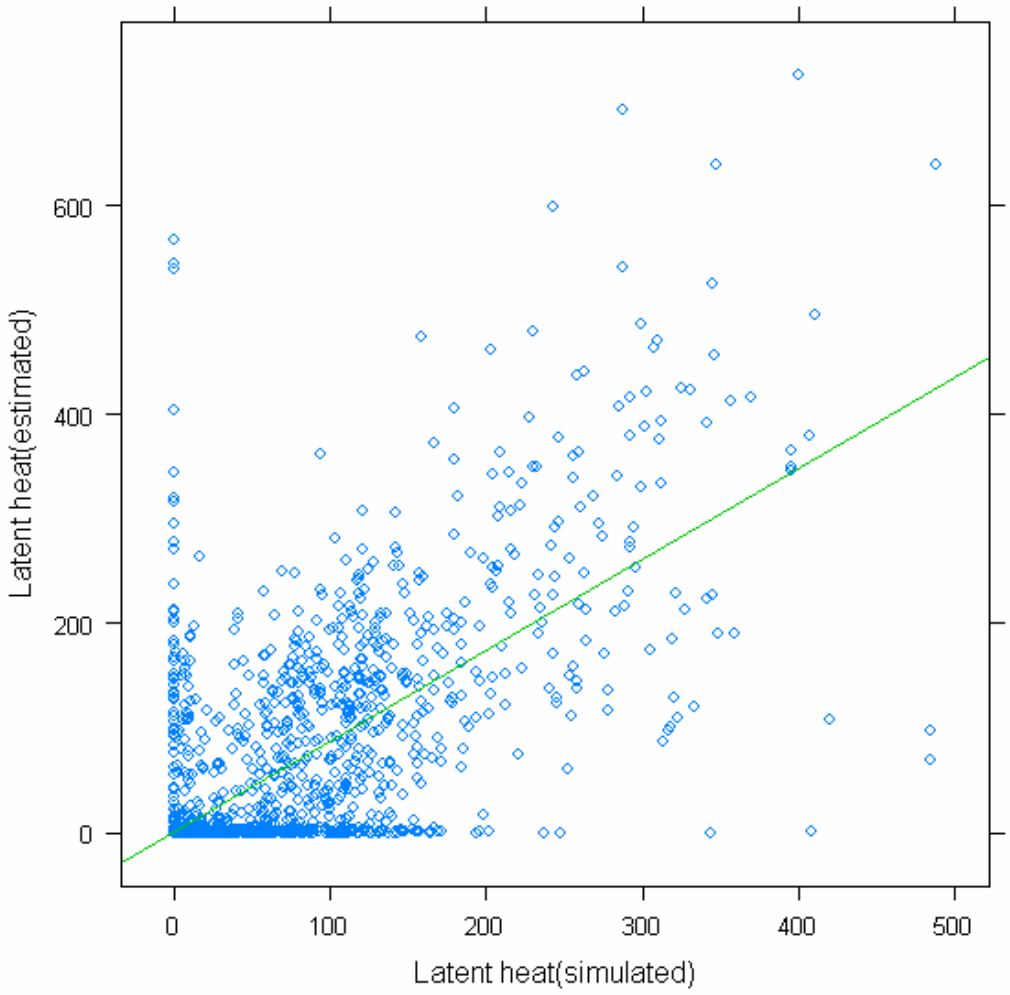

Fig. 7 Scatter plot of Estimated Latent heat for DoY 86-92, giving regression coefficient (R^2) of 0.49 (green line indicates line of best fit)

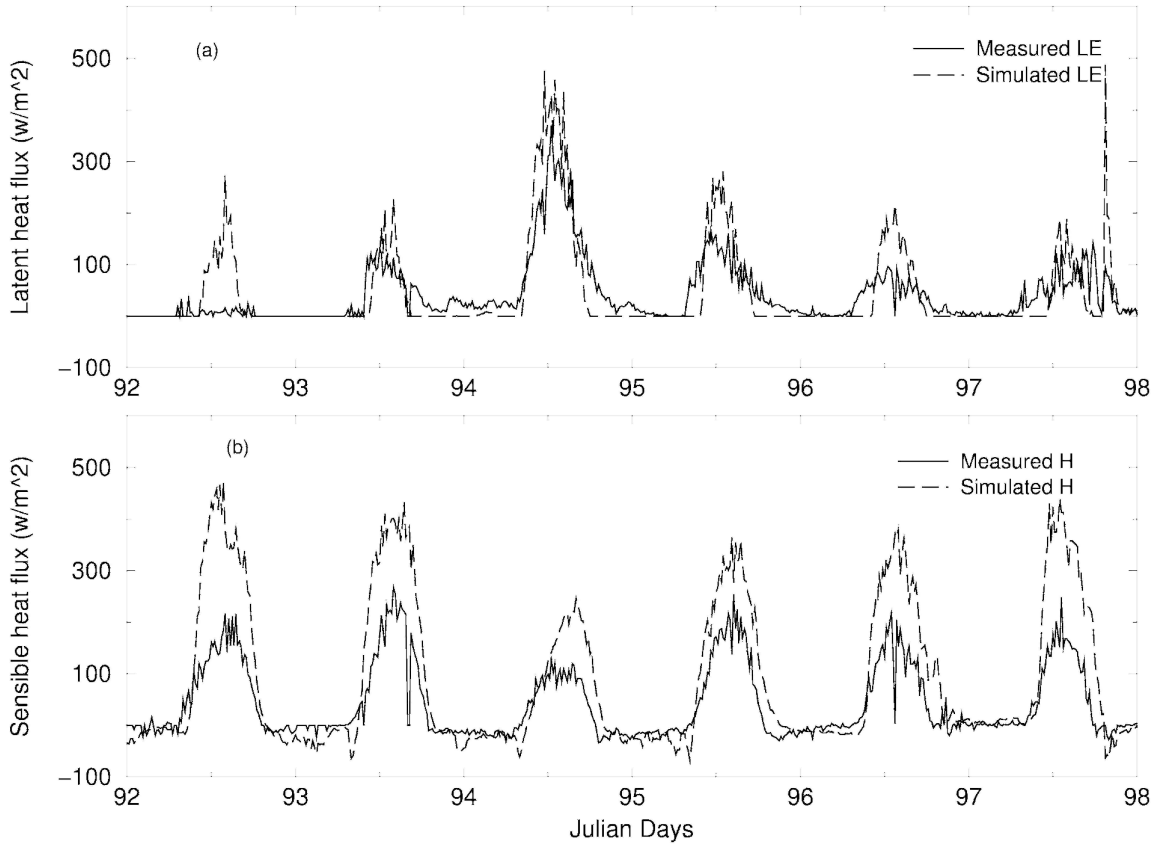

Fig.8. Comparison of diurnal variation of latent heat flux (a) and sensible heat flux (b) between simulation and observation on days 92-98

Soil moisture

Three different comparisons are discussed in this section: 1) comparison of simulated soil moisture in the superficial layer, which corresponds to 10 cm, with soil moisture measured at the depth of 4 cm; 2) simulated soil moisture in the middle layer, which corresponds to 35cm, compared against measured moisture at the depth of 24 cm, taken as an average of the estimated moisture measured at 16 and 32 cm and 3) simulated soil moisture in a deeper layer, corresponding to 1m depth, compared with measured soil moisture at the depth of 1m.

The model is able to reproduce the diurnal variability of soil surface moisture [Fig. 9a], with each moisture peak being associated with the rainfall events in the superficial layer. The root mean square error between simulation and observation for superficial soil layer is 0.033. However, the result indicates that soil surface tends to lose more moisture than observation, underestimating the measured soil moisture. The differences may be attributed to the degree by which specified soil porosity represent actual conditions at the site, error in specification of certain soil parameters in the model, and also the uncertainty characterized in the precipitation forcing. The possible error in specification of soil properties, in particular, hydraulic diffusivity, is addressed in the sensivity study in next section. The model, in its current form, does not accommodate soil property heterogeneities with depth. The effective porosity used for the application was the constant value of 0.4 (taken as an average of measurements recorded from the six samples). Camiera et al. (2005) have indicated that different soil sampling methods can cause compaction, destroying soil macro-porosity, especially in the ploughed layer. The soil porosity also decreases with depth due to compaction, and development of macro pores by biological activity near the surface

(Dingman, 2002). Since this was an agricultural site, the superficial soil porosity could have been different than deeper horizons. The averaged simulated soil moisture was 0.08 with a standard deviation of 0.03, and averaged estimated soil moisture was 0.108 with standard deviation of 0.01 for superficial layer for days 92 to 98.

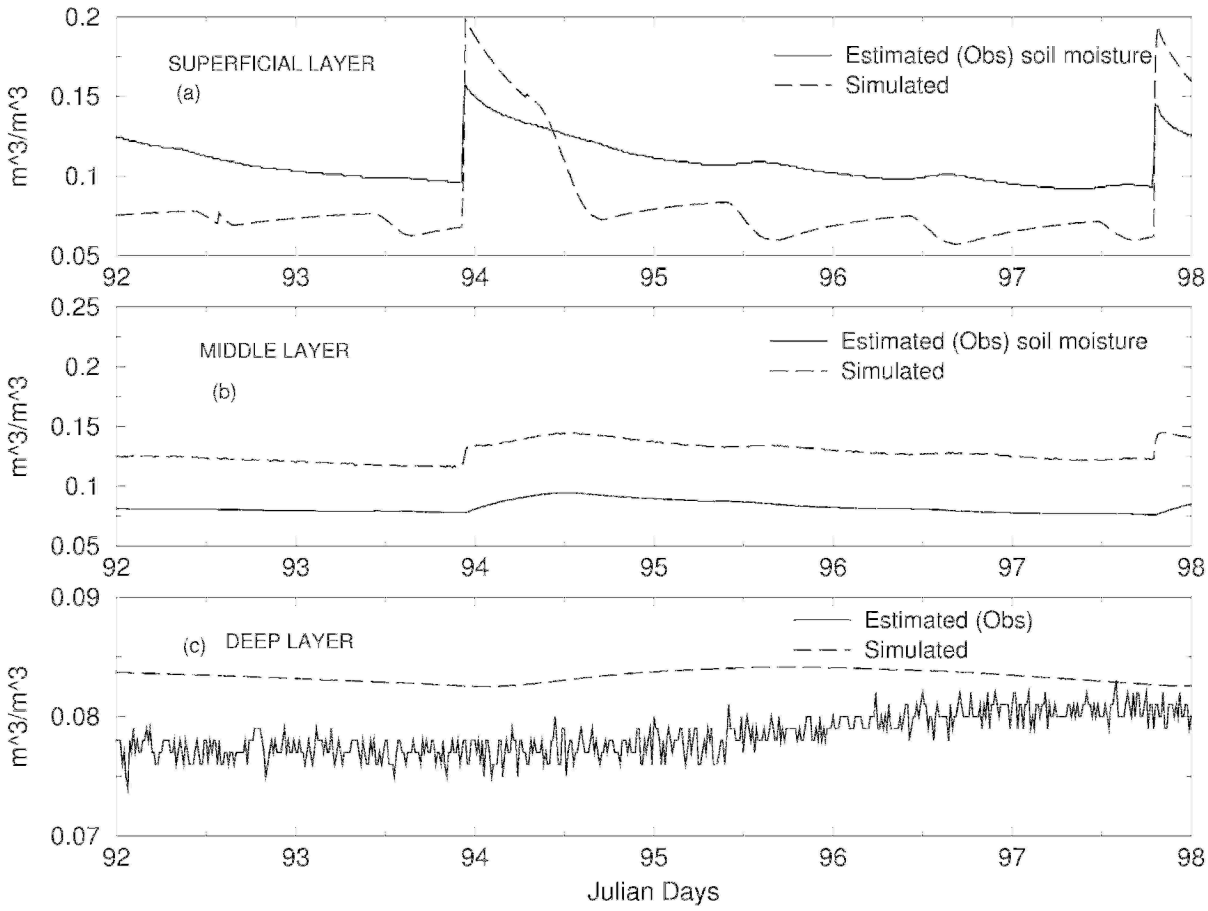

Fig. 9 Comparison of observed and simulated soil moisture in superficial layer (a), middle layer (b), and deeper layer (c) for days 92-98; differences are within measured uncertainty ($\pm$ 0.05 m^3/m^3)

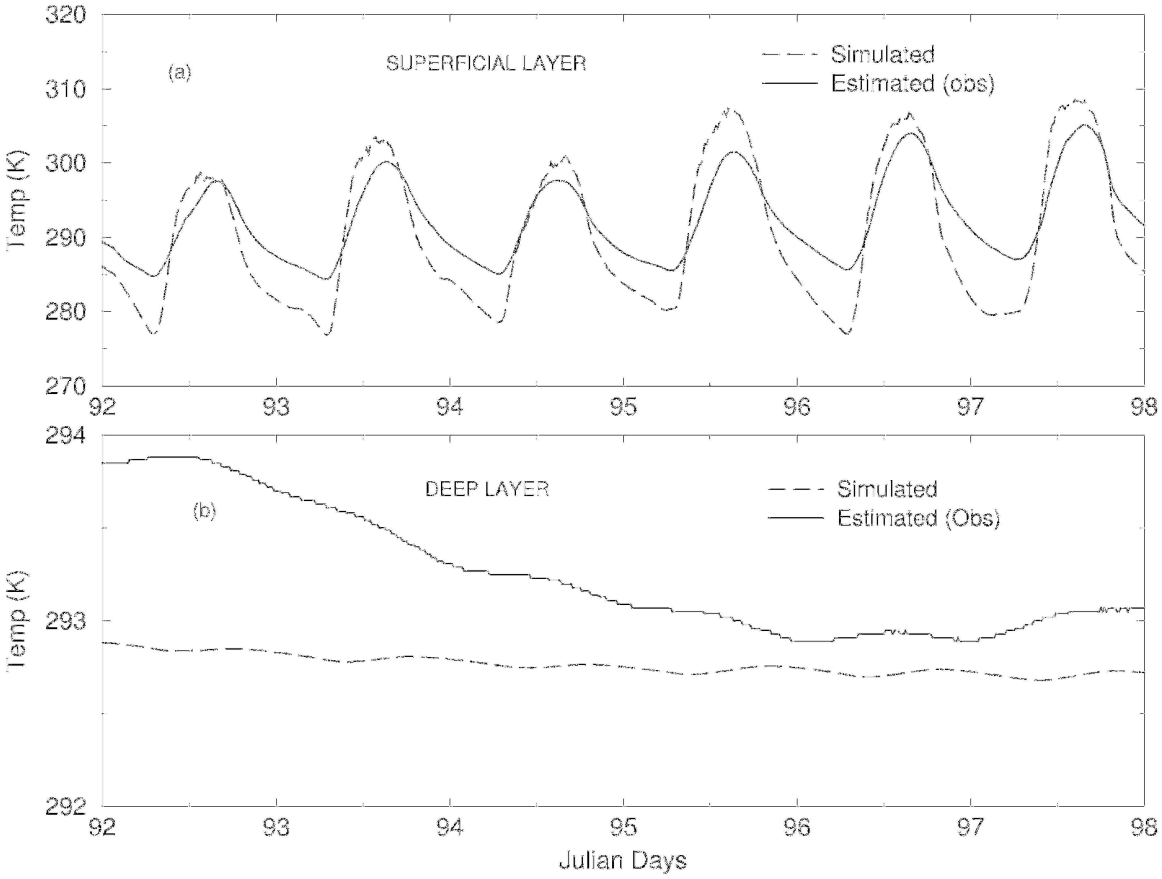

Fig. 10 Comparison of observed and simulated soil surface temperature in surface (a) and deeper layers (b) for days 92-98

Figures 9(b) and 9(c) represent comparisons between simulated soil moisture in the middle layer and observed soil moisture and simulated soil moisture in a deeper layer and observed soil moisture respectively for the days 92 to 98. The averaged simulated and observed soil moisture for the middle layer is 0.08 and 0.13 respectively, with root mean square error of 0.04 for those days. The mean simulated and observed soil moisture for the deeper layer is 0.07 and 0.08 respectively with root mean square error of 0.005.

Overall, the comparison shows that the model can reproduce diurnal variability of the soil moisture in all superficial, middle and deep layers. Moreover, correct precipitation is critical for correct simulation of the soil moisture; in particular predicting soil moisture peaks. This uncertainty produces more limitations in evaluating the diurnal cycle of photosynthesis.

Soil temperature

The diurnal variation of temperature differences was studied for two different depths: 1) superficial layer of 10 cm and 2) deeper layer of 1m. Figures 10(a) and (b) compares simulated temperature with observed temperature in the superficial layer and deeper layer respectively.

Both simulated and observed soil surface temperature vary with the same period, indicating that the superficial soil temperature simulation is able to reproduce the diurnal variation of soil surface temperature. The root mean square error is 5.06 K with mean simulated and estimated soil surface temperature being 292.33K and 290.17K respectively. The root mean square error for the deep soil temperature simulation with the observation is 0.57K with mean simulated and observed deeper soil temperature being 293.25K and 292.76K. The simulation in deep layer showed a strong diurnal variation, which is unusual at

the depth of 1m. As noted by Campbell and Norman (1998), the amplitude and phase of this temperature variation depends on the relative vertical position, and constituent properties, such as thermal diffusivity, heat capacity and density. This was the motivation for another sensivity study with respect to thermal diffusivity, which will be discussed in the following section.

5.2 Model Sensitivity to Thermal diffusivity and Hydraulic Diffusivity

We recognized that model simulations, in general can be affected by error in specification of the physical parameters, as discussed in Section 5.1. In particular, in the absence of field data, we relied on the literature, to infer some of the parameters, including thermal diffusivity and hydraulic diffusivity that best conform to soil properties in the field. To address this concern, sensitivity analysis to thermal diffusivity and hydraulic diffusivity was conducted, while keeping all other boundary conditions and physical forcing constant in the model. The purpose of these sensitivity studies was to investigate model behavior to thermal diffusivity and water diffusion coefficient.

Thermal diffusivity [L^2T^{-1}] is the ratio of thermal conductivity to volumetric heat capacity, C* (latter described in eqn 2), and hence an important parameter for determining ground heat flux. Thus, thermal diffusivity linearly correlates with thermal conductivity.

Several studies have been conducted to demonstrate sensitivity of energy fluxes and soil temperature to the soil thermal conductivity. The thermal conductivity of soil decreases as the saturation level in the soil increases. Kersten (1949) found that thermal conductivity is related to the logarithm of the moisture content. The Fourier amplitude sensitivity test to quantify sensitivity of fluxes indicated that while stomatal conductance and surface roughness account for most of the variance in the fluxes, under conditions of large heat conduction into

the soil, soil thermal conductivity exhibits an important control over the sensible heat flux (Collins and Avissar, 1994). On the other end, hydraulic diffusivity or diffusion coefficient is a critical parameter in soil water movement and it increases with water content. Flow due to pressure gradient is expressed as the product of the diffusion coefficient and water content gradient (Darcy's law, Dingman, 2002). Jacquemin and Noilhan (1990) have emphasized that soil moisture diffusivity regulates delivery of soil moisture from deep layers to the surface, and then influences the evaporation.

For this analysis, two different values of thermal diffusivity, $5*10^{-7}$ m^2/s and $5*10^{-8}$ m^2/s are used and three different values of diffusion coefficient (D_c) [L^2T^{-1}] (described in eqn 19a and 19b), 10^{-7}, 10^{-8}, and 10^{-9} are used. Our sensitivity study indicates that both latent heat and sensible heat fluxes appear to be consistent with different values of thermal diffusivity (Fig. 11 and Fig. 12), indicating less heat conduction in the soil. Figures 13, 14 and 15 illustrate that the soil moisture and surface temperature difference for different values of thermal diffusivity are smaller in magnitude. This partially explains why the differences in energy fluxes are smaller. However, the deep soil temperature response to thermal diffusivity is significant (Fig. 16). The deep soil temperature simulation with lower thermal diffusivity of 10^{-7} m^2/s shows strong diurnal variation. The mean square error between estimated and simulated deep soil temperature is 0.61 K and 0.55 K using thermal diffusivity of 10^{-7} and 10^{-8} m^2/s respectively. Our results indicated that deep soil temperature was most sensitive to the thermal diffusivity and lower order of thermal diffusivity produces least error in the current application.

Figures 13 and 14 illustrate the difference in soil moisture simulation, in superficial (13 a & b); middle (13c); and deeper (14) layers, from the estimated soil moisture in both

middle and deeper soil layers. The difference is least with the lowest value of diffusion coefficient of 10^{-9} m^2/s. As a response to precipitation in mid-day on Julian day 94 (Fig. 6), the soil moisture in the superficial layer peaks considerably higher than estimated with lower diffusivity values of 10^{-9} m^2/s. The mean square error between the simulation and estimated is 0.042 m^3/m^3, while the mean square error for the simulation with diffusivity of 10^{-8} m^2/s and 10^{-7} m^2/s are 0.04 m^3/m^3 and 0.033 m^3/m^3 respectively. As a consequence of soil moisture availability, the surface evaporation is reduced, increasing surface temperature for day 94 with the lowest magnitude of diffusivity compared with the estimation (Fig. 15 a & b). The simulations appear to be consistent for different values of diffusivity for days 92-96 except for days 94, 97 and 98. The mean square errors between simulation and estimation are 5.31K, 5.25K and 5.07K for hydraulic diffusivities of 10^{-8} m^2/s and 10^{-7} m^2/s respectively. The deeper soil temperature simulation does not seem to respond to changes in diffusion coefficients for lower thermal diffusivity (Fig. 16a). The differences observed in the deeper soil temperature simulation with higher thermal diffusivity are also smaller, although the lowest diffusivity produces a least error (Fig. 16b), indicating that deeper soil temperature simulation is more sensitive to the change in thermal diffusivity than hydraulic diffusivity. The sensible heat flux shows a similar variation as superficial soil temperature simulation, as could be predicted based on the linear relationship of sensible heat flux with soil surface temperature (Fig.12), with RMSE of 116.53 W/m^2, 116.61 W/m^2 and 99.55 W/m^2 using diffusivity coefficient of 10^{-9} m^2/s, 10^{-8} m^2/s and 10^{-7} m^2/s respectively. Figure 11 illustrates non-linear change of simulated latent heat as response to change in surface temperature for different values of hydraulic diffusivity. The RMSE between simulated and estimated is

calculated as 71.91 W/m^2, 70.17 W/m^2 and 55.14 W/m^2 using diffusivity coefficients of 10^{-9} m^2/s, 10^{-8} m^2/s and 10^{-7} m^2/s respectively.

The overall sensitivity study indicates that energy fluxes, soil temperature and moisture respond differently to both diffusion coefficients, with deep soil temperature being most sensitive to the hydraulic diffusivity specified in the model.

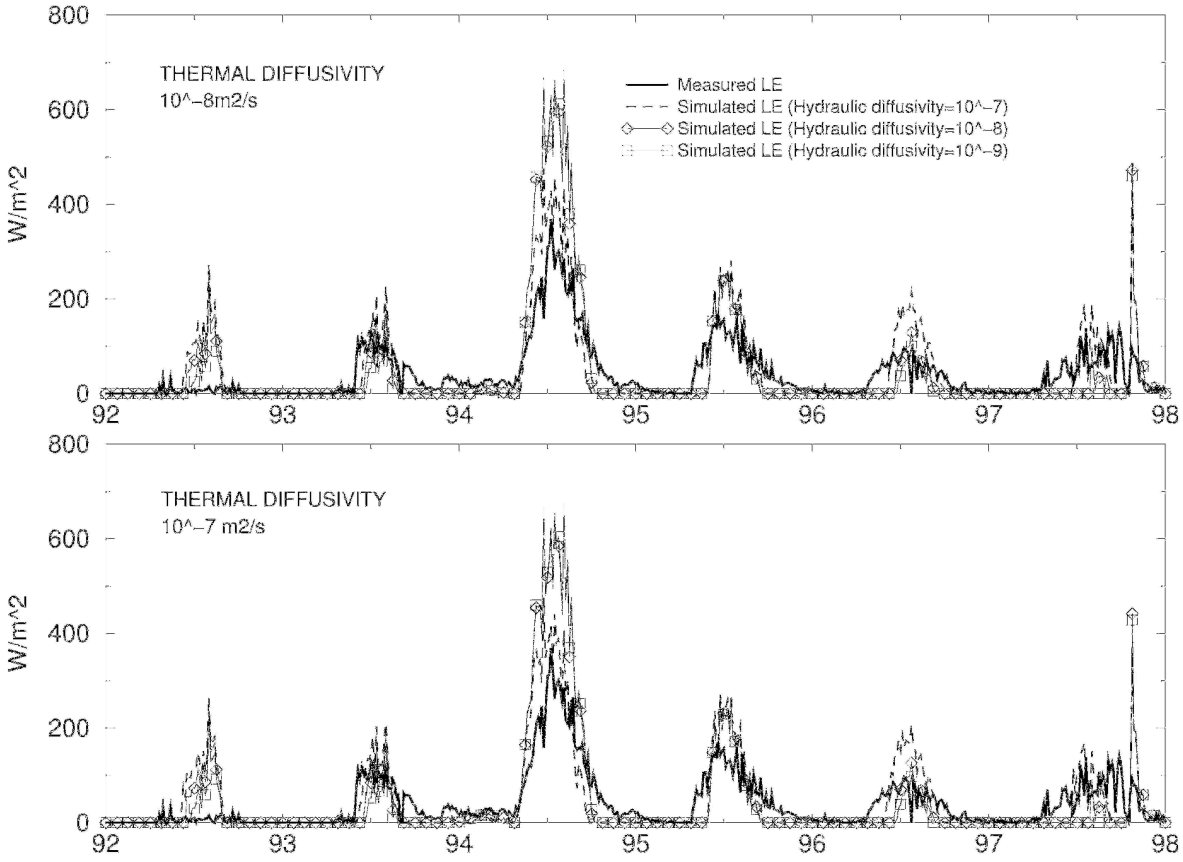

Fig. 11 Comparison of estimated and simulated latent heat flux to different values of diffusion coefficient and thermal diffusivity (a) Thermal diffusivity=10^{-8} m^2/s; and (b) Thermal diffusivity=10^{-7} m^2/s, for days 92-98.

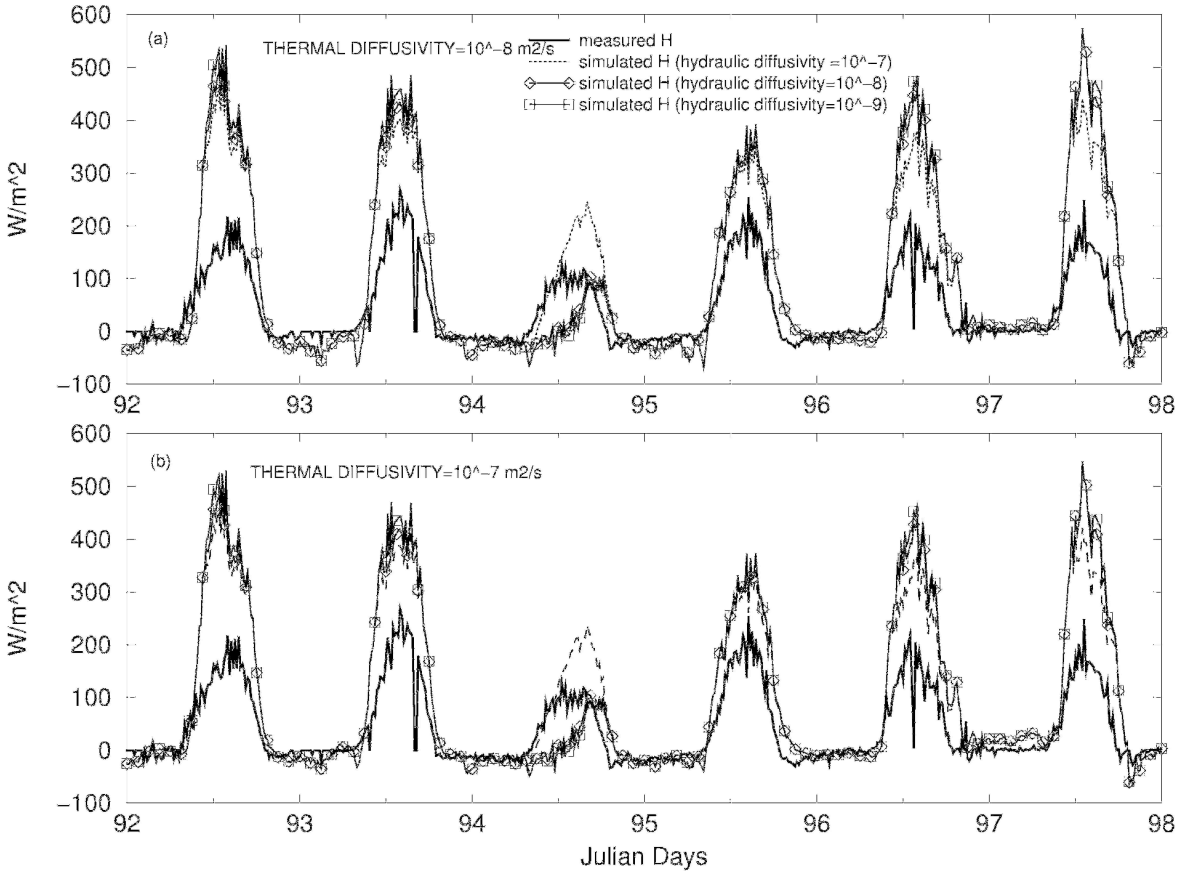

Fig.12. Comparison of estimated and simulated sensible heat flux to different values of diffusion coefficient and thermal diffusivity (a) Thermal diffusivity=10^{-8} m^2/s; and (b) Thermal diffusivity=10^{-7} m^2/s, for days 92-98.

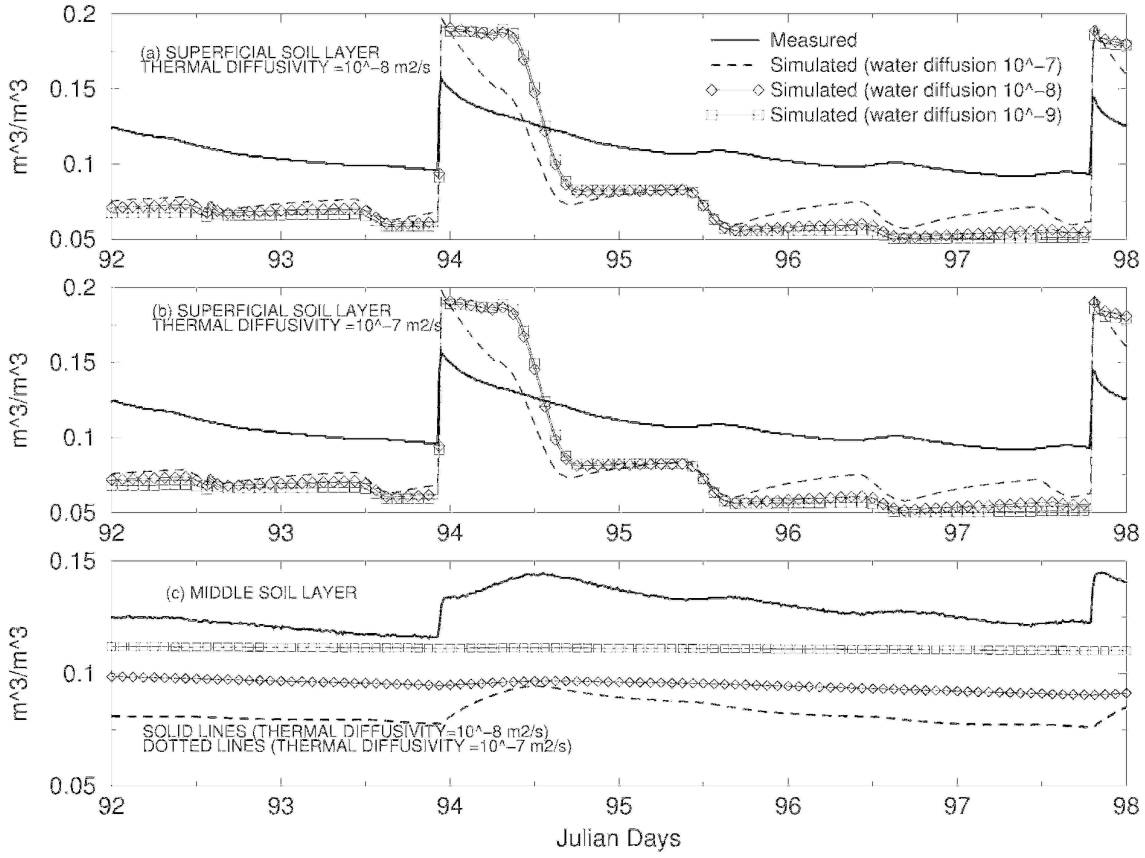

Fig.13. Comparison of estimated and simulated soil moisture for different values of diffusion coefficient and thermal diffusivity in (a) superficial soil layer with thermal diffusivity=10^{-8} m^2/s; and (b) Thermal diffusivity=10^{-7} m^2/s; (c) middle soil layer, for days 92-98.

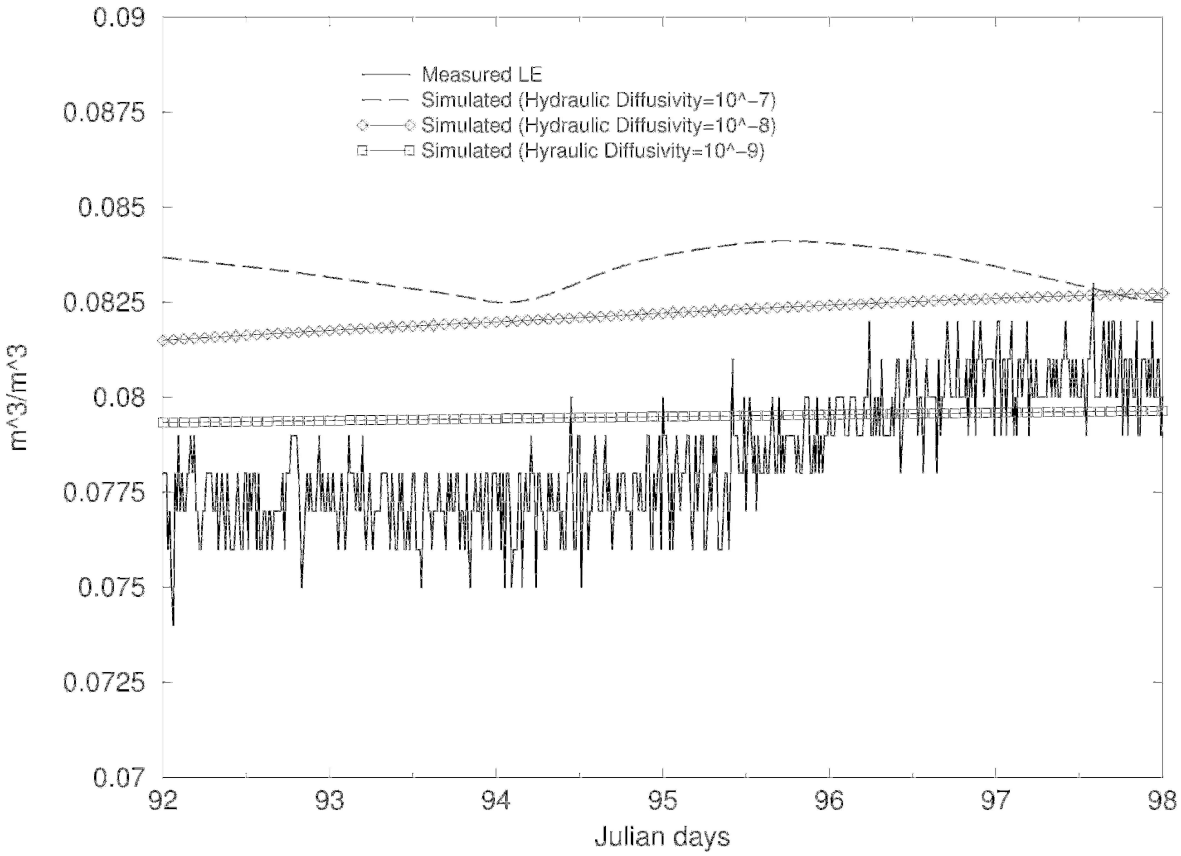

Fig.14. Comparison of estimated and simulated deep soil moisture to different values of hydraulic diffusivities

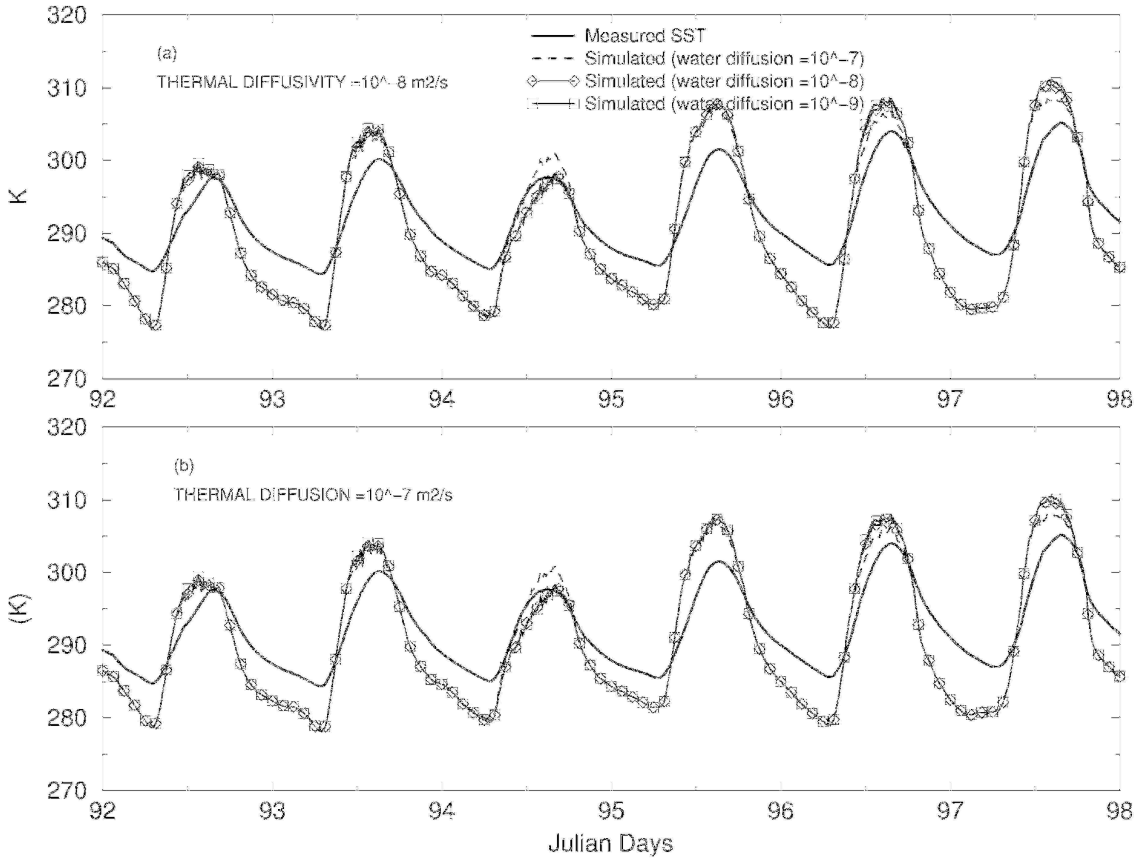

Fig.15. Comparison of estimated and simulated soil surface temperature to different values of diffusion coefficient and thermal diffusivity (a) Thermal diffusivity=10^{-8} m^2/s; and (b) Thermal diffusivity=10^{-7} m^2/s, for days 92-98.

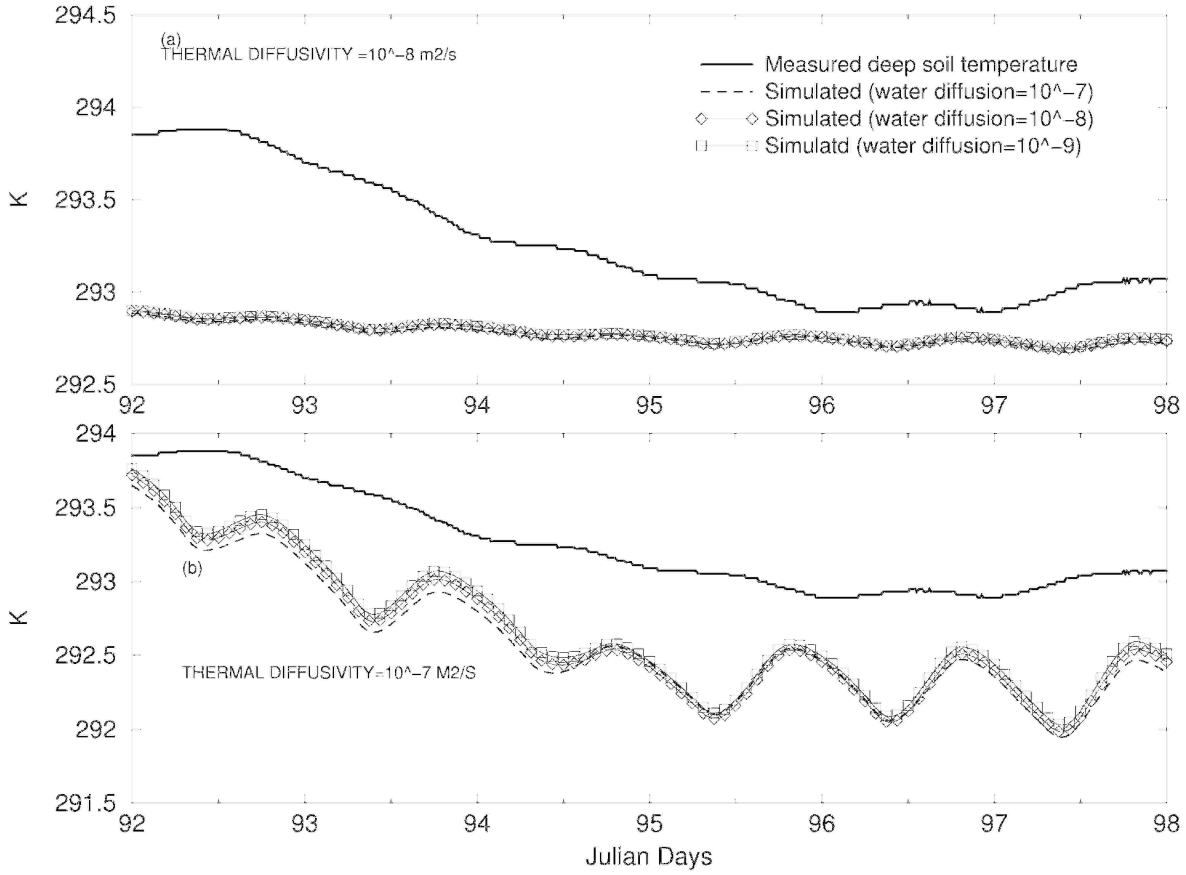

Fig.16. Comparison of estimated and simulated deep soil surface temperature for different values of diffusion coefficient and thermal diffusivity (a) Thermal diffusivity=10^{-8} m^2/s; and (b) Thermal diffusivity=10^{-7} m^2/s, for days 92-98, showing its sensitivity to thermal diffusivity.

6. CONCLUSIONS

We used a land surface hydrology model to understand the diurnal cycle of land atmosphere interactions in an irrigated agricultural field in Florida. Model results were compared against field observations and estimates.

Our analysis showed that the model is able to characterize the diurnal energy fluxes for the early growing season of corn with pronounced diurnal maximum of latent heat and sensible heat fluxes in the midday, as expected. Net radiation is partitioned to 3% of ground heat flux, for the early growing season. The large discrepancy between the model simulation and field estimations on energy fluxes can be largely explained by the uncertainty in the forcing data, both precipitation and radiation, and eddy-covariance estimates of energy fluxes. On the other hand, diurnal soil moisture and temperature responses to precipitation and radiation seem to be captured well by the model. The difference, that exists, may be attributed in part to the current application's inability to capture soil property heterogeneities as a function of depth and error in specification of soil parameters but it is within measurement uncertainty. In the absence of field data, we relied on the literature, to infer some of the parameters, including thermal diffusivity and hydraulic diffusivity. To address this concern, sensitivity analysis to thermal diffusivity and hydraulic diffusivity was conducted, while keeping all other boundary conditions and physical forcing constant in the model. As opposed to previous applications with the model (at larger field scales and not for agricultural fields), it was found that thermal diffusivity and hydraulic diffusivity have a strong impact on the partitioning of the surface energy fluxes.

This work underscores the importance of forcing data for evaluating model physics, hence improving the understanding of diurnal land atmosphere interactions, in response to precipitation and irrigation, in an irrigated agricultural field.

7. REFERENCES

1. Barros, A.P. *Adaptive Multilevel modeling of land-atmosphere interactions.* Journal of Climate, 8, pp 2144-2160, 1995.
2. Brooks, R.H. and Corey, A.T. *Hydraulic properties of porous media.* Hydrology Paper 3, Colorado State University, Fort Collins, CO, pp 27-110, 1964.
3. Campbell, G.S. *A simple method for determining unsaturated conductivity from moisture retention data.* Soil Sci. 117, pp 311-314, 1974.
4. Campbell, G.S. and Norman, J.M. *An introduction to Environmental Biophysics.* New York: Springer-Verlag, 2nd Ed, 1998.
5. Casanova, J., Lin, T., Jang, M., Tien K., Judge, J., Lanni, O. and Miller, L. *Field Observations During the second microwave water and energy balance experiment (MicroWEX-2): from March 17 through June 3, 2004*. Center for Remote Sensing, The University of Florida, 2005
6. Cameira, M.R., Fernando, R.M., Ahuja, L.R. and Pereira, L. 2005. *Simulating the fate of water in field soil-crop environment for evaluating management effects on water quality and crop production*. Journal of Hydrology, 315, pp 1-24, 2005.
7. Ciach, G.J. *Local random errors in tipping-bucket rain gauge measurements*. Journal of Atmospheric and Oceanic Technology, 20, pp 752-759, 2003.
8. Collins, D. and Avissar, R. *An evaluation with the Fourier amplitude sensitivity test (FAST) of which land-surface parameters are of greatest importance for atmospheric modeling*. Journal of Climate, 7, pp 681-703, 1994.
9. Devonec, E. and Barros, A.P. *Exploring the transferability of a land-surface hydrology model*. Journal of Hydrology, 265, pp 258-282, 2002.

10. Dingman, S.L. *Physical Hydrology*, Prentice-Hall, Inc., 2nd Edition, 656 pp, 2002.
11. Eagleson, P.S. *Climate, soil and vegetation: Introduction to water balance dynamics*. Water Resources Research, 14, No. 5, pp 705-712, 1978.
12. ECMWF. *ECMWF forecast model physical parameterization.* Research Manual 3, ECMWF Research Department, UK, 1991.
13. Falkenmark, M. *Society's interaction with the water cycle: a conceptual framework for a more holistic approach.* Hydrological Sciences, 42, pp 451-466, 1997.
14. Garcia-Quijano, J.F. and Barros, A.P. *Incorporating canopy physiology into a hydrology model: photosynthesis, dynamic respiration and stomatal sensitivity.* Ecological Modeling, 185, pp 29-49, 2005.
15. Gebremichael, M. and Barros, A.P. *Evaluation of MODIS Gross Primary Productivity (GPP) in tropical monsoon regions*. Remote Sensing of Environment, 100, pp 150-166, 2005.
16. Gutmann, E.D. and Small, E.E. *The effect of soil hydraulic properties vs. soil texture in land surface models.* Geophysical research letters, 32, L02402, 2005.
17. Halls, F.G. and Sellers, P.J. *First International Satellite Land Surfaced Climatology Project (ISLSCP) Field Experiment (FIFE) in1995*. Journal of Geophysical Research, 100, Issue D12, pp 25383-25396, 1995.
18. Hornebuckle, B.K. and England, A.W. *Diurnal Variation of Vertical Temperature Gradients within a Field of Maize: Implications for Satellite Microwave Radiometry*. IEEE Geosciences and Remote Sensing Letters, 2, No 1. 2000

19. Jacquemin, B. and Noilhan, J. *Sensitive study and validation of a land surface parameterization using the HAPEX-MOBILHY data set*. Earth and Environmental Science, 52, No. 1, pp 93-134, 1990.
20. Kahan, D.S., Xue, Y. and Allen, S.J. *The impact of vegetation and soil parameters in simulations of surface energy and water balance in the semi-arid Sahel: A case study using SEBEX and HAPEX sahel data*. Journal of Hydrology, 320, pp 238-259, 2006.
21. Kersten, M.S. *Laboratory research for the determination of the thermal properties of soils*. Research Laboratory Investigations, Engineering Experimental Station, Technical Report 23, 1949.
22. Korner, C., Scheel, J.A., and Bauer, H. *Maximum leaf diffusive conductance in vascular plants*, Photosynthetica, 13, pp 45-82, 1979.
23. Louis, J.F. *A parametric model of vertical eddy fluxes in the atmosphere*, Boundary layer Meteorol. 17, pp 187-202, 1979.
24. Mahrt, L. and Sun, J. *The subgrid velocity scale in the bulk aerodynamic relationship for spatially averaged scalar fluxes.* Monthly weather Rev. 123, pp 3032-3041, 1995.
25. Massman, W.J. and Lee, X. *Eddy covariance flux corrections and uncertainties in long term studies of carbon and energy balance*. Agriculture and Forest Meteorology 113, pp 121-144, 2002.
26. Rawls, W.J. and Brakensiek, D.L. *Prediction of soil water properties for hydrologic modeling.* Watershed Mgmt Eighties, ASCE, pp 293-299, 1985.
27. Rowntree, P.R. *Atmospheric parameterization schemes for evaporation over land; basic concepts and climate modeling aspects.* Proceedings of Workshop/Fall School

on Measurement and Parameterization of Land-Surface Evaporation Fluxes, Banyuls, Springer, Berlin, pp. 5-29, 1991.

28. Schwartz, B.E. and Bozart, L.F. *The Diurnal variability of Florida rainfall.* American Meteoro. Society, Vol. 107, pp 1535-1545, 1979.
29. Sellers, P.J. *Modeling and observing land-surface-atmosphere interactions on large scales.* Survey in Geophysics, 12, pp 85-114, 1991.
30. Stewart, J.B. *Modeling surface conductance of pine forest.* Agri. Forest Meteoro. 43, pp 17-35, 1998.
31. Winter, T.C. *Uncertainties in estimating the water balance of lakes.* Water resources Bulletin 17, pp 82-115, 1981.
32. Xu, M., Chen. J. and Qi, Y. *Growing season temperature and soil moisture along a 10 km transect across a forested landscape*. Climate Research, Vol 22, pp 57-72, 2002.
33. Yildiz, O. *Assessment and simulation of hydrologic extremes by a physically based spatially distributed hydrologic model*. Ph.D. Thesis, The Pennsylvania State University, University Park, PA, 2001.
34. Yildiz, O. and A. P. Barros. *Climate Variability and Hydrologic Extremes-Modeling the Water and Energy Budgets in the Monongahela River Basin*. Climate and Hydrology in Mountain Areas, De Jong, Colins and Ranzi (Eds.), Wiley (Pub.), pp 303-318, 2005.
35. Zhang, Y., Liu, C.,Yu, Q., Shen, Y., Kendy, E., Kondoh, A., Tang, C. and Sun, H. Energy flux and Priestley–Taylor parameter over winter wheat and maize in the North China Plain. Hydrological processes, 18, pp 2223-2234, 2004.

8. APPENDIX

APPENDIX 1: LSHM Schematic of major energy and water fluxes [Adapted from Devonec & Barros, 2002]

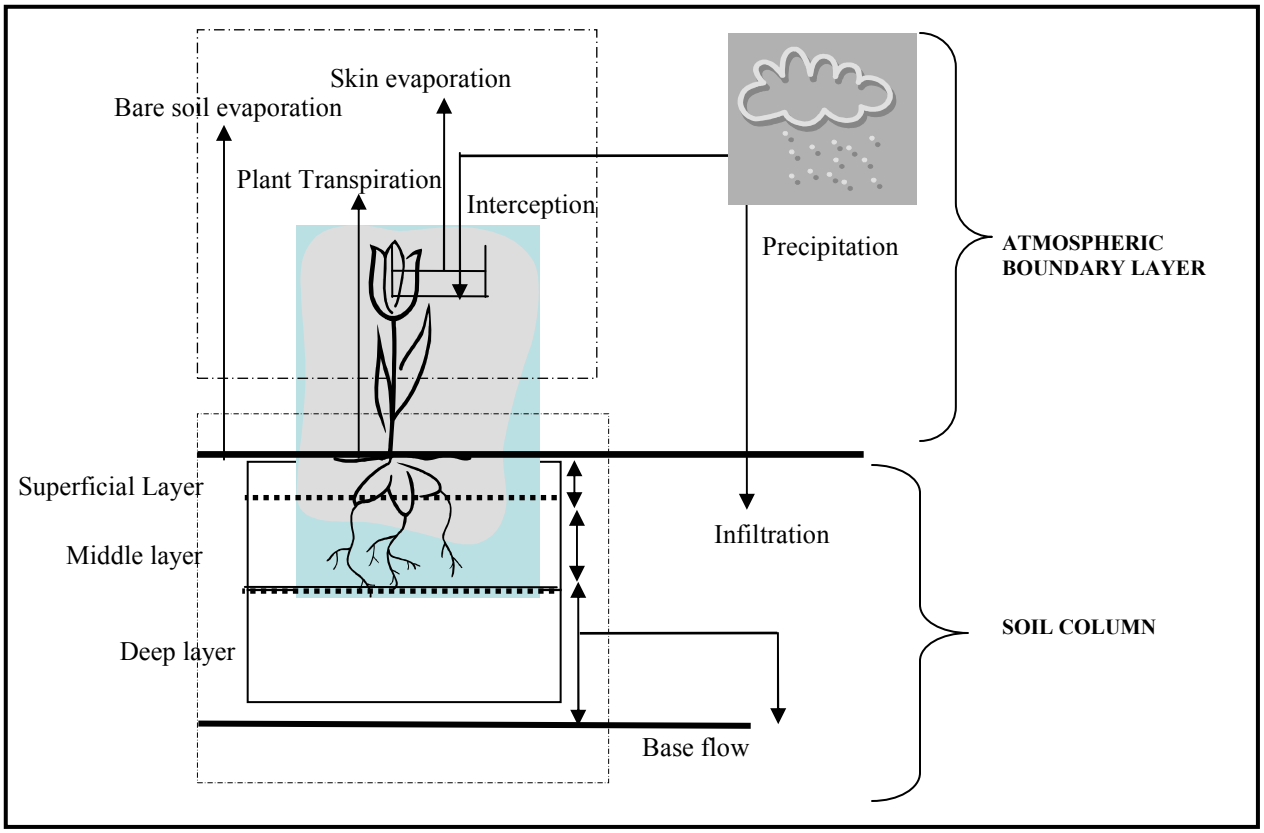

APPENDIX 2: Flowchart of the land surface hydrology model

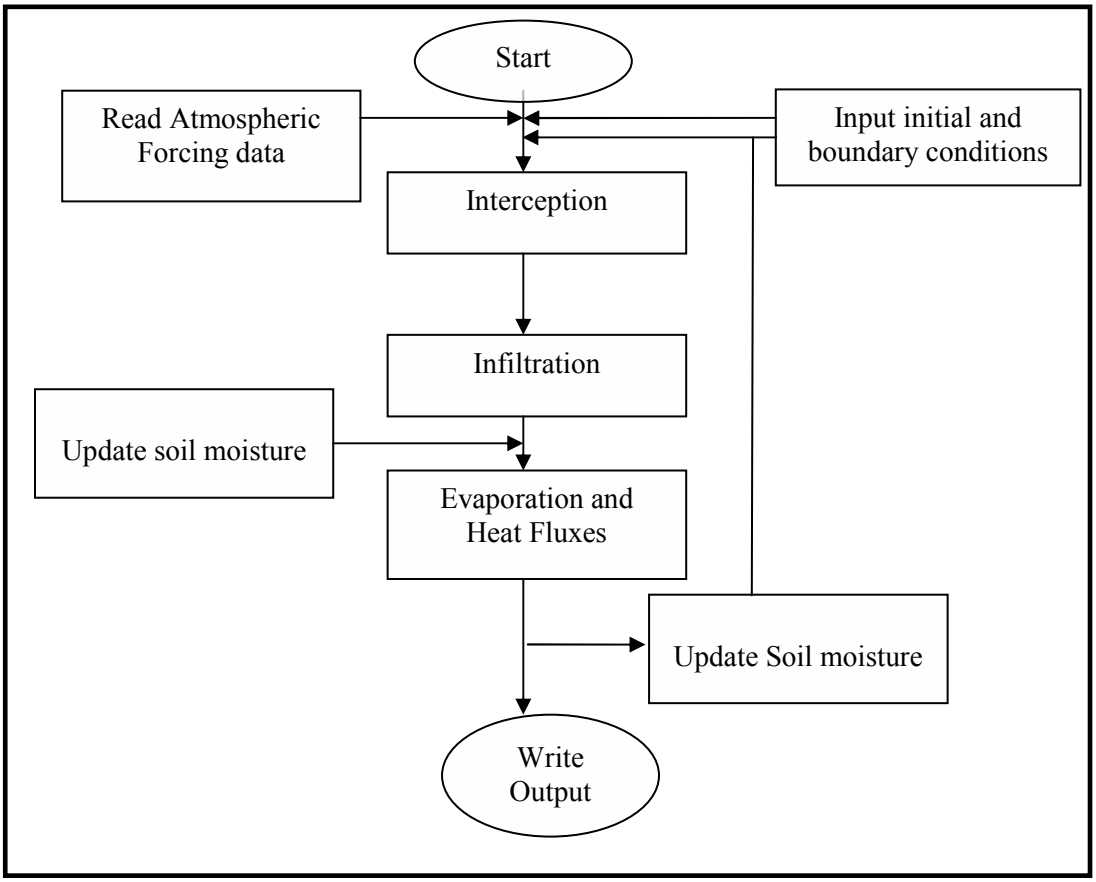

APPENDIX 3: Site Map in Citra, Florida, showing different soil point features

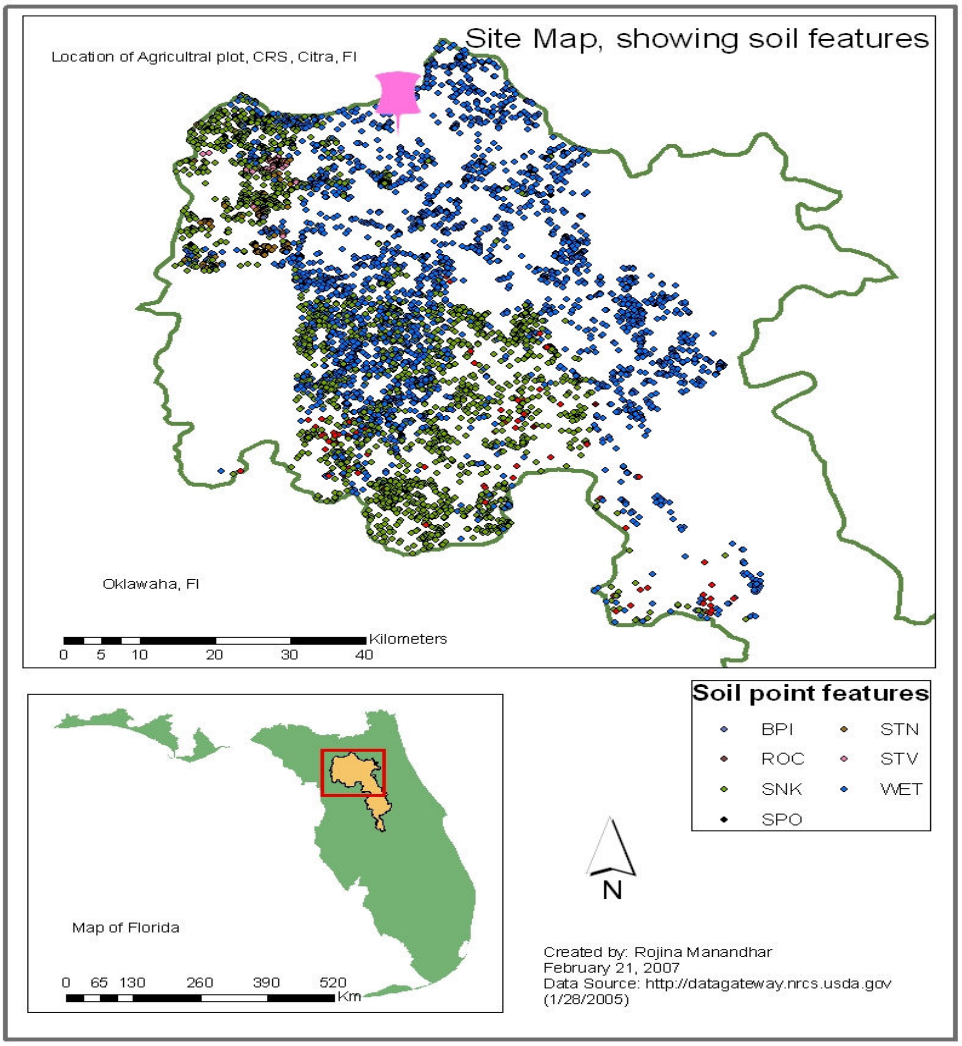

Soil point feature description [Datagateway, NRCS, USDA, 2005]

BPI (Borrow Pit): material have been removed, usually for construction purposes. Typically .25 to 3 acres.

GUL (Gully): A small channel with steep sides cut by running water through which water ordinarily runs only after a rain, or after ice or snow melts.

ROC (Rock Outcrop): An exposure of bedrock at the surface of the earth. Typically .25 to 2 acres.

SLP (Short steep slope): Narrow soil area that has slopes that are at least two slope classes steeper than the slope class of the surrounding map unit.

SNK (Sinkhole): A closed depression formed either by solution of the surficial rock or by collapse of underlying caves. Typically .25 to 3 acres.

SPO (Spoil area) : A pile of earthy materials, either smoothed or uneven, resulting from human activity. Typically .25 to 3 acres.

STN (Stony Spot): A spot where 0.01 to 0.1 percent of the surface cover is rock fragments that are greater than 10 inches in diameter in areas where the surrounding soil has no surface stones. Typically .25 to 2 acres.

STV(Very stony spot): A spot where 0.1 to 3 percent of the surface cover is rock fragments that are greater than 10 inches in diameter where the surrounding soil has less than 0.01 percent of the surface cover of stones. Typically .25 to 2 acres.

WET (Wet spot): A somewhat poorly drained to very poorly drained area that is at least two drainage classes wetter than the named soils in the surrounding map unit. Typically .25 to 2 acres.

APPENDIX 4: Field layout showing location of sensors and rain gages (Casanova et al. 2005)

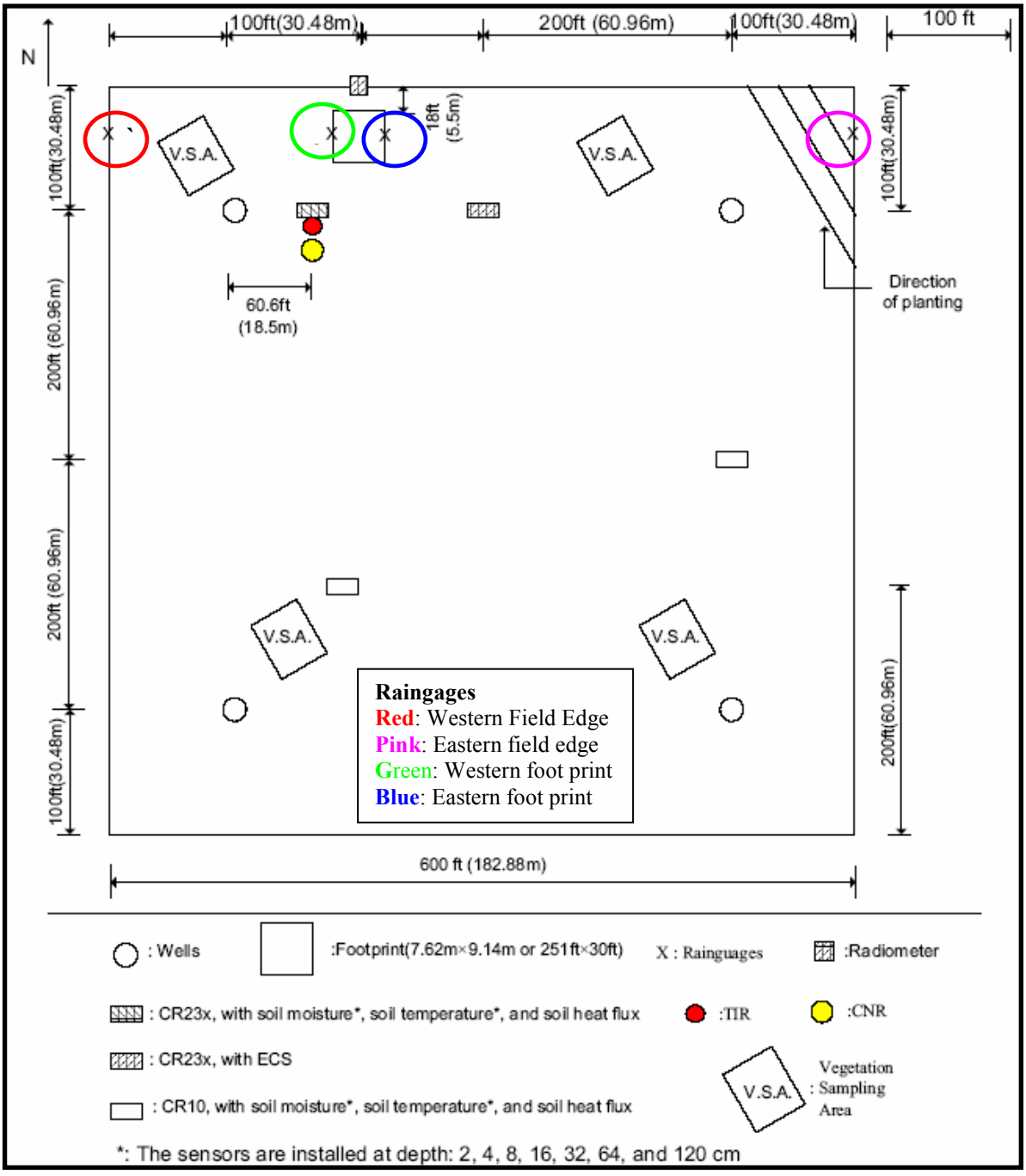

APPENDIX 5(a): Parameters values for forcing the model or estimating fluxes in the model

Parameter	Description	Value	Unit	Source
a	Albedo	0.25		Averaged value, calculated from observed short wave radiation (in and out)
C_p	Specific heat capacity of air	1010	J/kgK	
hmeasure	Measurement height	2.1	m	Observed/measured
z_{veg}	Vegetation height	1	m	Maximum height observed
dish	Displacement height	0.7	m	[calculated as $0.7*z_{veg}$]
rcmin	Minimum stomatal resistance	40	sm^{-1}	Korner, 1979
	Elevation of the surface	20	m	Measured
zref	Aerodynamic roughness height	0.1	m	Estimated
zrefs	Aerodynamic roughness height for heat	0.02	m	Estimated
zrefl	Aerodynamic roughness height for moisture	0.02	m	Estimated

APPENDIX 5(b). Soil parameters for forcing the model (Loamy sand)

Parameter	Description	Value	Unit	Source
c	Heat capacity of soil	$24*10^5$	$Jkg^{-1}K^{-1}$	
ds_0	Superficial layer	0.1	m	Estimated for the model
ds_m	Middle layer	0.35	m	Estimated for the model
ds_p	Deep layer	1.00	m	Estimated for the model
wilt	Wilting point	0.05	m^3 m^{-3}	Handbook of hydrology
w_{fc}	Field capacity	0.14	m^3 m^{-3}	Handbook of hydrology
k_h	Saturated hydraulic conductivity	$3.8*10^{-4}$	ms^{-1}	Observed (average value recorded for six samples)
TD	Thermal diffusivity	$2*10^{-7}$	m^2s^{-1}	Averaged for sand and clay
D_c	Hydraulic diffusivity			
WCS	Effective porosity	0.25	m^3 m^{-3}	Observed
sf	Wetting front suction (Green and Ampt parameter of wetting front soil suction head)	7.17	m	Calculated using Green-Ampt model [Dingman, Physical Hydrology]
power	Power used in unsaturated hydraulic conductivity equation	3.28		Devonec and Barros [2002]
	Soil emissivity	0.94 or 0.98		0.94 estimated for corn field, 0.98 estimated for wet sand